A national laboratory of the U.S. Department of Energy
Office of Energy Efficiency & Renewable Energy

National Renewable Energy Laboratory

Innovation for Our Energy Future

Smart Sensor System for Structural Condition Monitoring of Wind Turbines

May 30, 2002 — April 30, 2006

M.J. Schulz
University of Cincinnati
Cincinnati, Ohio

M.J. Sundaresan
North Carolina A&T State University
Greensboro, North Carolina

Subcontract Report
NREL/SR-500-40089
August 2006

NREL is operated by Midwest Research Institute • Battelle Contract No. DE-AC36-99-GO10337

Smart Sensor System for Structural Condition Monitoring of Wind Turbines

May 30, 2002 — April 30, 2006

M.J. Schulz
University of Cincinnati
Cincinnati, Ohio

M.J. Sundaresan
North Carolina A&T State University
Greensboro, North Carolina

NREL Technical Monitor: A. Laxson
Prepared under Subcontract No. XCX-2-31214-01

Subcontract Report
NREL/SR-500-40089
August 2006

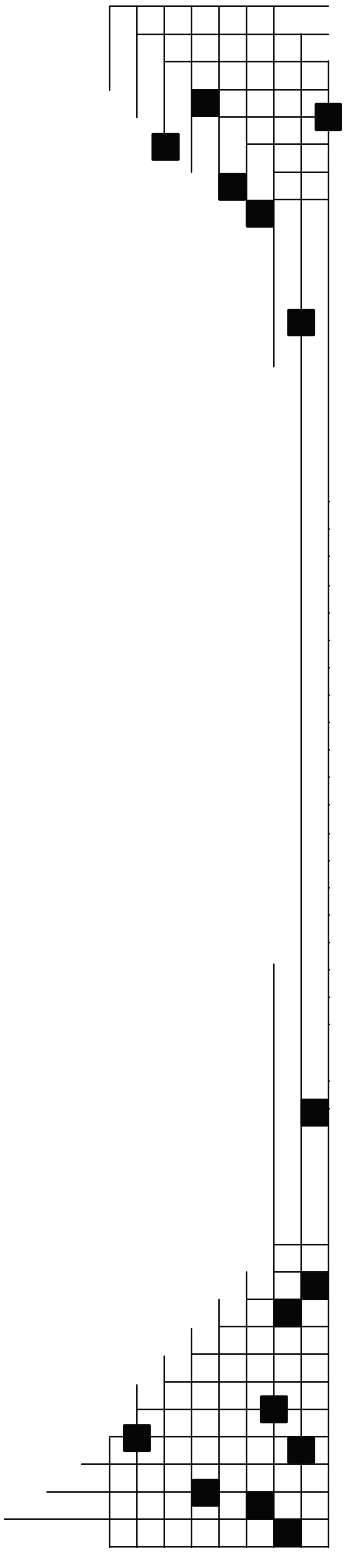

National Renewable Energy Laboratory
1617 Cole Boulevard, Golden, Colorado 80401-3393
303-275-3000 • www.nrel.gov

Operated for the U.S. Department of Energy
Office of Energy Efficiency and Renewable Energy
by Midwest Research Institute • Battelle

Contract No. DE-AC36-99-GO10337

NOTICE

Available electronically at http://www.osti.gov/bridge

Available for a processing fee to U.S. Department of Energy
and its contractors, in paper, from:

U.S. Department of Energy
Office of Scientific and Technical Information
P.O. Box 62
Oak Ridge, TN 37831-0062
phone: 865.576.8401
fax: 865.576.5728
email: mailto:reports@adonis.osti.gov

Available for sale to the public, in paper, from:

U.S. Department of Commerce
National Technical Information Service
5285 Port Royal Road
Springfield, VA 22161
phone: 800.553.6847
fax: 703.605.6900
email: orders@ntis.fedworld.gov
online ordering: http://www.ntis.gov/ordering.htm

This publication received minimal editorial review at NREL

Printed on paper containing at least 50% wastepaper, including 20% postconsumer waste

Contents

Figures

Executive Summary

The high cost of energy due to limited resources may be the most critical problem facing the world today, and this problem is becoming worse each year. The energy crisis is focusing a lot of attention on renewable energy, such as wind and solar energy, which is not likely to run out. In the case of wind energy, there is great interest in deploying small and large wind turbines for generating distributed power for residential and rural areas. These turbines represent a significant capital investment for the owner and the turbine must operate for up to 30 years. Failure of one rotor blade on the turbine could cause catastrophic damage and jeopardize the user's investment and confidence in wind energy. Structural health monitoring (SHM) of the rotor blades is a solution that can warn of damage to the blade and protect the entire horizontal-axis wind turbine from failure. In addition, a condition-based maintenance program can be adopted using the health monitoring information. The advantages of structural health monitoring and a condition based maintenance strategy are to:

- Minimize labor costs for inspection of turbines.
- Prevent unnecessary replacement of components based on time of use.
- Uncover design weaknesses before failure.
- Improve the availability of power while preventing overload of the turbine.
- Allow repair rather than replacement of blades by detecting damage early.
- Protect the investment in wind power by residential owners, utility companies, and public facilities such as schools that are trying to reduce energy costs.
- Use lighter advanced blades made from fiberglass and graphite that will allow the large turbines to react to wind changes more quickly, and thus capture more wind energy.

The design of the wind turbine blade is an important factor in the performance (power produced) and reliability of the wind turbine. The trend in blade design is toward complex blade shapes to improve aerodynamic efficiency, and the use of combined fiberglass graphite, and balsa wood materials to improve strength and reduce the blade mass moment of inertia that will result in increased “wind capture.” In other words, blade geometry and materials are becoming high-tech and complex, and structural over-design of the blade is no longer an an acceptable approach. The push to increase wind turbine performance and maintain reliability is driving a need for installation of low-cost continuous health monitoring systems on wind turbine blades. This system could provide critical information about the location and propagation of blade damage. If a blade fails, the rotor can become unbalanced, which can destroy the entire turbine. Wind turbine blades made of composites have sudden audible AEs during damage growth. This means that instruments can be affixed to the blades to detect and locate these emissions to prevent blade failure. Monitoring the blade for damage is also useful in static testing to determine at what location the blade starts to fail. This information can be used to improve blade design and manufacturing. Wind turbine blades are mostly composite structures with complex geometry, large size, and sections that are built of different materials. Any sensor system to be used on the blades must be low cost, simple, and operate over decades of use. This makes developing a practical SHM system for wind turbine blades a real challenge.

In this project, the Intelligent Mechanisms Laboratory at North Carolina A&T State University and the Smart Materials Nanotechnology Laboratory at the University of Cincinnati collaborated to develop a structural neural system (SNS) for SHM of wind turbine blades. The National Renewable Energy Laboratory (NREL) sponsored the work and engineers from Sandia National Laboratories provided guidance. The tasks that were performed to produce the prototype SNS include:

- Modeling and simulation of damage in composite materials.
- Developing continuous sensors for use in the sensor system.

- Developing the signal processing system.
- Developing a methodology for buckling health monitoring.
- Developing damage assessment, prognosis, and life extension techniques.
- Fabricating a working sensor system.
- Testing this system on a wind turbine blade at NREL.

The SNS that was developed is based on AE monitoring, which is a practical approach for low-cost SHM of large composite structures such as wind turbine blades. The main advantage of the SNS is that many sensor elements can be used with only 2-4 channels of data acquisition. This tremendously simplifies SHM. Furthermore, the method is passive, which means no pre-damage data or diagnostic waveforms are needed.

The SNS was tested to identify damage initiation and propagation on a 9-meter-long wind turbine blade during a static proof test to failure at the NREL test facility in Boulder, Colorado. The testing was performed in January 2006 with the help of the NREL and Sandia Labs staff. Two configurations of the SNS were tested. The first configuration used continuous sensors connected to a commercial AE monitoring system. The second configuration used continuous sensors connected to the full SNS developed in the project. The test instrumentation was brought to NREL from NCA&TSU and the Univ. of Cincinnati. Piezoelectric wafers were bonded onto the surface of the wind turbine blade and interconnected to form continuous sensors that were connected to the commercial data acquisition systems or the SNS processor built in the project. AE data were recorded during the test until the blade failed. The testing produced some interesting conclusions. In the beginning of the testing, after the blade settled and concurrent AEs quieted, damage initiated in one location on the blade. Then, as the load was increased, damage started in a second, third, and fourth location until finally there was a catastrophic buckling failure of the blade caused by the graphite spar cap delaminating from the fiberglass shear web of the load bearing rib in the blade. The SNS indicated the general area where the damage started and indicated how damage progressed, which is valuable information for blade design and for verifying the manufacturing technique. Strain gages on the blade did not provide a clear indication of damage until the skin buckled. The blade failed at a load above the design load.

The results of laboratory testing and the blade testing at NREL provide confidence that SHM of large composite structures that have complex geometry and are made of multiple materials is practical using a simple and low-cost SNS. Based on the testing, recommendations to improve the SNS for application on wind turbine blades include using a finer grid pattern of the neurons, locating neurons inside the blade at critical locations such as the rib and joints, and setting the neuron firing parameters based on the structure underneath each neuron to help pinpoint the damage locations. There are also several technical upgrades to the hardware of the SNS that could be pursued as subsequent projects to increase the number of neurons to monitor large structures, and to have the SNS wirelessly transmit data from a rotating system to the fixed frame. In the future, the SNS could also be reconfigured for health monitoring of other components on wind turbines, such as bearings and gears. In addition, the architecture of the SNS may be modified for measuring other variables, such as the pressure distribution on the blade. This information can be used in the control system to improve efficiency and prevent overload and fatigue of the blade. This project was highly successful because it developed the SNS, which is a new approach for health monitoring of composite structures that is practical and sensitive. We predict that future wind turbines will become “smart” and use sensors to diagnose their health and also to define structural performance limits that can be fed back to a control system to prevent damage from occurring. The high-tech SNS developed for wind turbine blades can also be configured for use on other types of composite materials – such as helicopter rotor blades, for example.

1.0 Introduction

Wind turbine blades are designed to have lifetimes of up to 30 years. These blades accumulate on the order of 10^9 load cycles and the fatigue life of the blade is an important design consideration. Wind turbine blades can become damaged by moisture absorption, fatigue, wind gusts, or lightning strikes. In wind farms, aerodynamic interaction between different turbines can cause unpredictable and excessive loads on the blades. These excessive loads accelerate fatigue damage to the blade. In addition, normal aerodynamic loads and loads that result from changing gravity moments cause fatigue damage to the blades. The blades are usually made from fiberglass, which is a cost-effective material for this application. However, because of the low specific modulus of fiberglass, the blade natural frequencies are low and the deflections of the cantilevered blade can be large. If a fatigue-damaged rotor blade fails, it can cause catastrophic damage to the wind turbine and possibly damage nearby structures or injure people. Predicting the exact fatigue life of a blade is difficult, and it is difficult to tell the extent of fatigue damage that might have occurred to a blade. Thus, manufacturers are seeking a method to continuously monitor the condition of the blade and warn of damage or impending failure.

Wind turbine blades sometimes fail near the root section or the third of the blade near the root. Buckling of the blade's surface at the maximum chord section is one type of failure. The blades may operate for a large number of cycles with little reduction in strength and elastic properties, and then damage may propagate quickly to failure. Health monitoring of the rotor blades and timely identification of potential failure areas can help prevent damage or failure of the horizontal axis wind turbine. A health monitoring system that is reliable, low cost, and integrated onto the blade may reduce wind turbine life-cycle costs and make wind energy more affordable. The structural health monitoring (SHM) information gathered could be used in a condition-based maintenance program that could minimize the time needed for inspection of components, prevent unnecessary replacement of components, prevent failures, and allow utility companies to be confident of power availability. In addition, SHM may allow the use of lighter blades that would provide higher performance with less conservative margins of safety. Furthermore, a wind turbine with lighter blades can respond to wind changes more quickly and capture more energy.

A SHM system to monitor wind turbine blades must be designed to consider thick structural sections, a complex built-up structure with multiple curvatures, and the use of a minimum number of signal processing channels. Various existing techniques including visual inspection, C-scan, AEs, Lamb wave propagation, and shearography can detect damage in composite blades. These techniques are labor intensive, or inaccurate, or difficult to use during operation, or require a large number of channels of data acquisition and storage of pre-damage data, or accessibility of the blade is required for an extended time. In this project, a new highly distributed continuous sensor concept that mimics the signal processing in the biological neural system was investigated. This approach can improve the level of sensitivity and lead to the development of a smart blade for continuous in-operation damage detection. One of the National Renewable Energy Laboratory's (NREL) concerns in the development of a smart blade is the cost of the sensor system. Because the piezoceramic sensor material is used for sensing high-frequency low-amplitude signals, little piezoelectric sensor material is used. The cost of the material and signal processing hardware would be justified by the increased reliability of the turbine. The smart blade could also provide blade response information to control the turbine performance and to increase the turbine's efficiency. The health monitoring system could monitor each blade on all turbines in a wind farm during operation. If damage is indicated, the particular turbine and blade could be identified and this information communicated to an operator through a diagnostic monitoring system. A damaged blade could be adjusted to reduce loads, or the turbine could be stopped for blade inspection and repair.

2.0 Modeling and Simulation of the Sensor System

A simulation is performed to aid in design of the sensor system. In the simulation to be described it is assumed that continuous sensors are used to form an array. Continuous sensors have multiple nodes connected in a series to one channel of data acquisition. The simulation of a 10 x 10 array sensor system is performed and the sensor system architecture used mimics that of a Structural Neural System (SNS). The SNS is briefly described. It consists of neurons of series-connected piezoceramic (PZT) nodes and is one possible concept for the arrangement of continuous sensors. The modeling and details of the simulation are given in references [1] and [2]. An impulse load is simulated at the center of a fiberglass panel that can represent cracking of fibers or an impact to the blade. The panel used for the simulation is 1.22 meters (m) square, 0.0064 m thick, and is modeled as being simply supported. A 10-by-10-m SNS shown in Figure 2.1 is used. The arrangement of the nodes on the panel is exactly symmetric. At the end of each neuron signal, processing electronics are shown as a small box in Figure 2.1. These units produce an output voltage for each neuron. The voltages are designated V1 through V20.

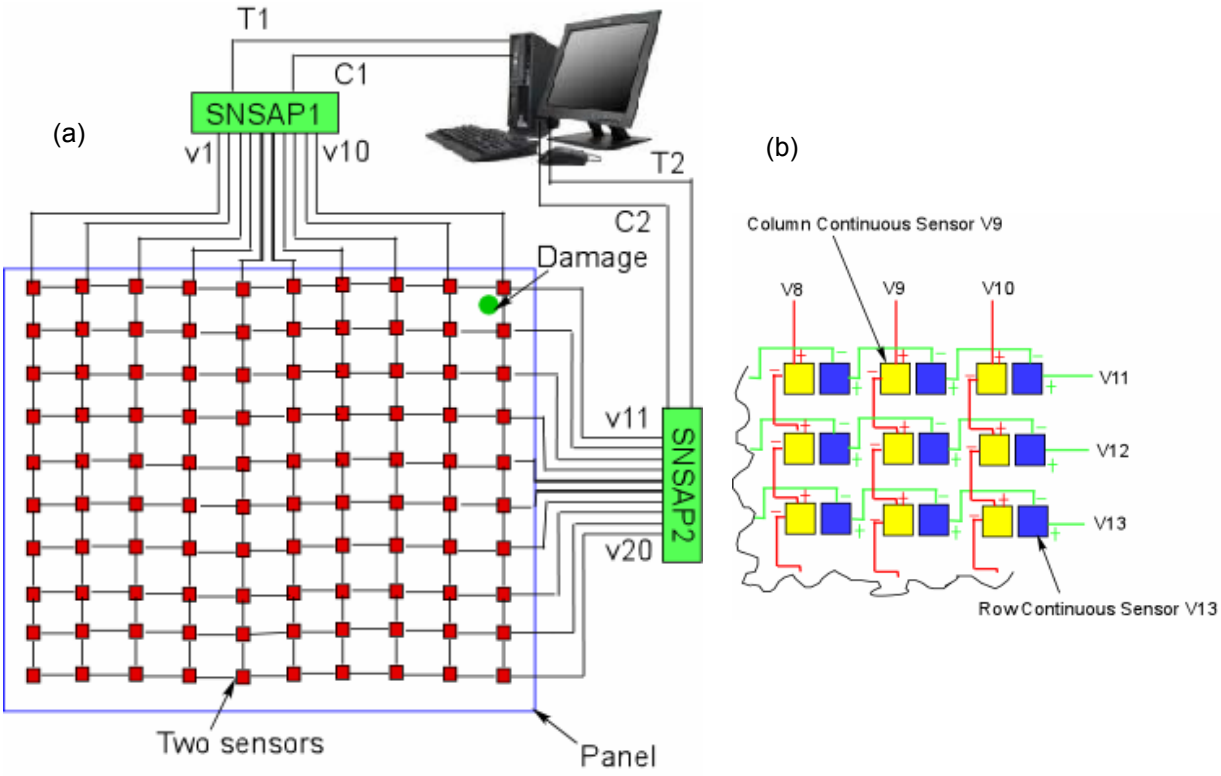

Figure 2.1. Architecture of the SNS: (a) Each small square indicates two adjacent sensor nodes. There are 200 sensors in (a). Circuits V1 through V20 contain 20 analog output signals from the continuous sensors. SNSAP1 and SNSAP2 are two analog processors built to simplify the damage location process. T1, C1, T2, and C2 are the four output signals sent to the computer. Software for damage detection is written using MATLAB and LABVIEW to acquire and analyze the data; (b) Zoomed version of (a) showing detail of arranging sensors to form row continuous sensors and column continuous sensors.

Following is a brief discussion of modeling of the electronic components representing the processing functions of the biological nerve cell. A neuron is formed by connecting the PZT sensor nodes in a series. A 1-M-ohm resistor signifying the resistance of an oscilloscope was connected to the output of each neuron, and each neuron signal is amplified by a factor of 10. A bridge rectifier was simulated by taking

the absolute value of the neuron signal, which produces only a positive rectified signal whenever the neuron voltage exceeds a 0.2-volt switching level. The absolute value of the signal, along with an on/off switch, models the characteristic of the bridge rectifier. The neurons are assumed to be connected in a series for this simulation. A large wave propagation simulation algorithm was developed for this purpose and can be used for any number of sensor elements and neurons. The excitation was located at the center of the plate. The loading considered in the simulation is an impulse input to represent a very high-frequency excitation, such as an acoustic emission (AE). The wave propagation response of the panel is shown in Figure 2.2. The time step used in computing the response is 1 microsecond and 200 vibration modes of the panel are used in computing the response solution. The 200th mode natural frequency is 452 kilohertz (kHz).

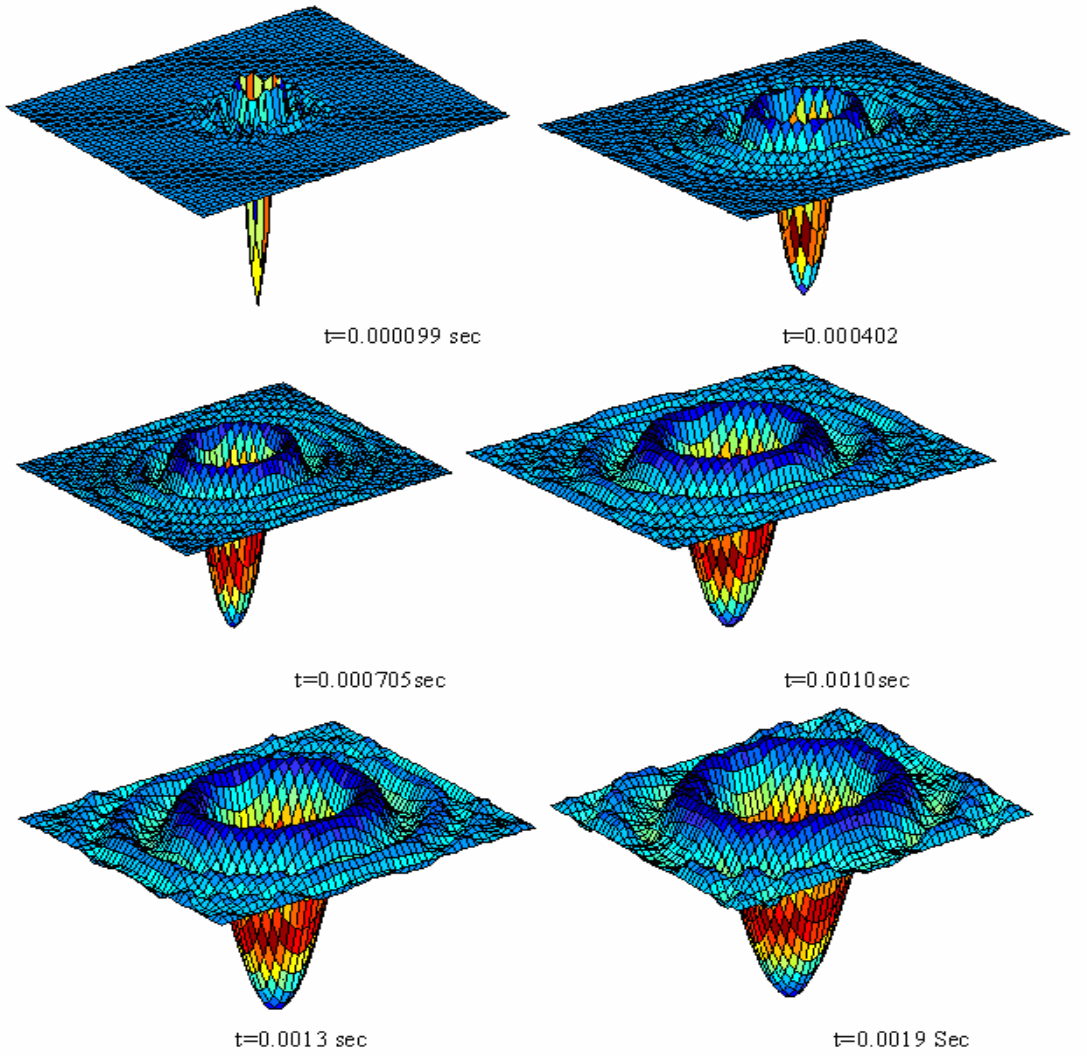

Figure 2.2. Response of the plate due to an impulse at the center of the plate.

Figure 2.3 shows the response of the plate for a simulated impulse excitation at the center of the simply supported glass fiber composite panel. The graph clearly indicates that the sensor is able to detect the high-frequency simulated excitation. The algorithm used to simulate the wave propagation assumes a linear solution and is efficient for design of the sensor system. The voltage output of all the 20 neurons is shown in Figure 2.3, but because of symmetry, half are exactly overlaid on each other.

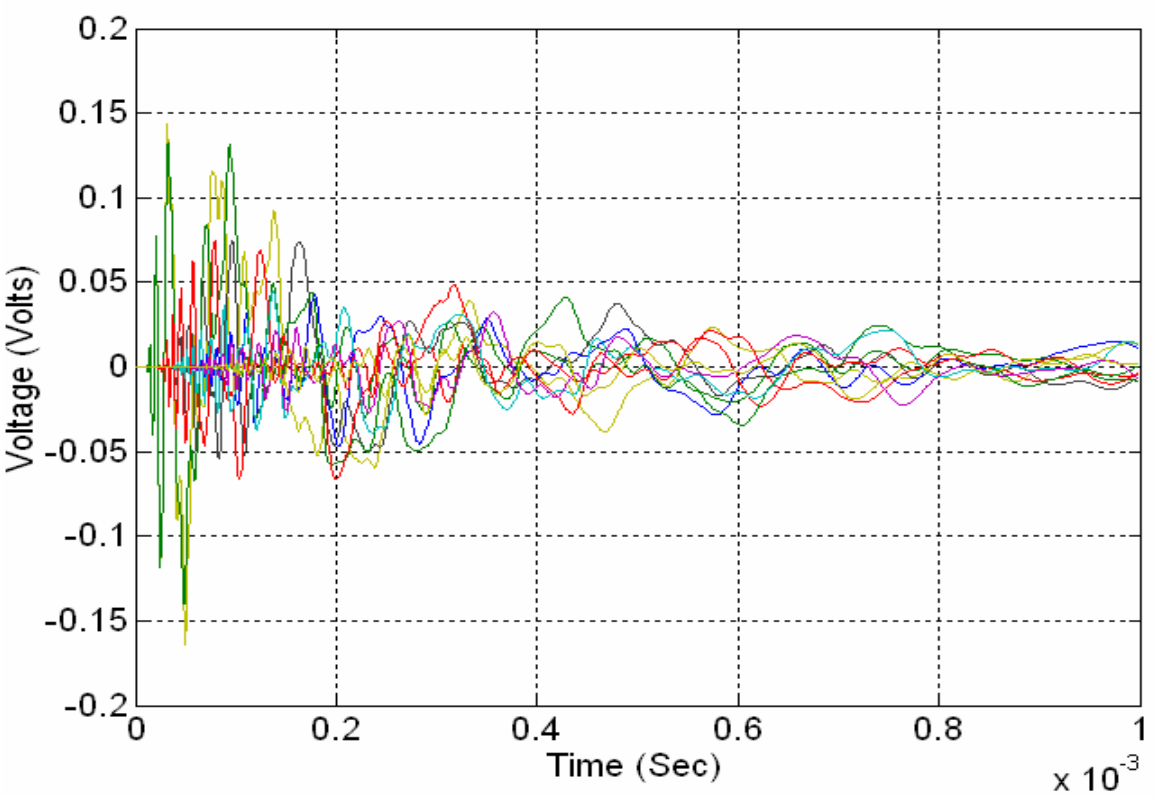

Figure 2.3. Simulation of the neuron responses due to an impulse (dirac delta function).

The sequential firing of the 10 column neurons is shown in Figure 2.4. The firing of the row neurons is not shown as they fire in the same order as shown for column neurons. The time of firing of the row neurons is the same as the column neurons because the plate used is a quasi-isotropic composite plate. In the initial part of the response, neurons 5 and 6 (Y-Neurons), and 15 and 16 (X-Neurons) are firing. The intersection of these row and column neurons is at the center of the panel. Later in the response the voltage output increases because the strain levels in the panel are increasing and because more modes are being strained. The output of the neurons adds together and the row and column output voltages increase due to the addition of all the neurons that are firing. Note that in the beginning of the response only two neurons are firing and later they all are firing. The symmetry in the panel causes the signals to overlap. These figures show that the SNS has located the source of an impact at the center of the panel by the intersection of the row and columns that are firing.

Figure 2.5 shows the response of each neuron after firing and indicates that the SNS has detected a very high-frequency signal and that the neuron corresponding to the color yellow has fired. The graph clearly indicates that a very high-frequency signal was recorded by the SNS and that later on a low-frequency signal dominates. The information in Figure 2.5 is actually reduced in the processor and is transparent to the user. These signals are combined into one row output and one column output.

The combined column outputs are shown in Figure 2.6. The column combined output is the signal recorded by the signal processing system. The amplitude of the initial part of the column of combined outputs also shows the high-frequency content and roughly indicates the level of damage caused by the fiber break or the impact. Typically, as damage propagated, the amplitude of the AE signals increased.

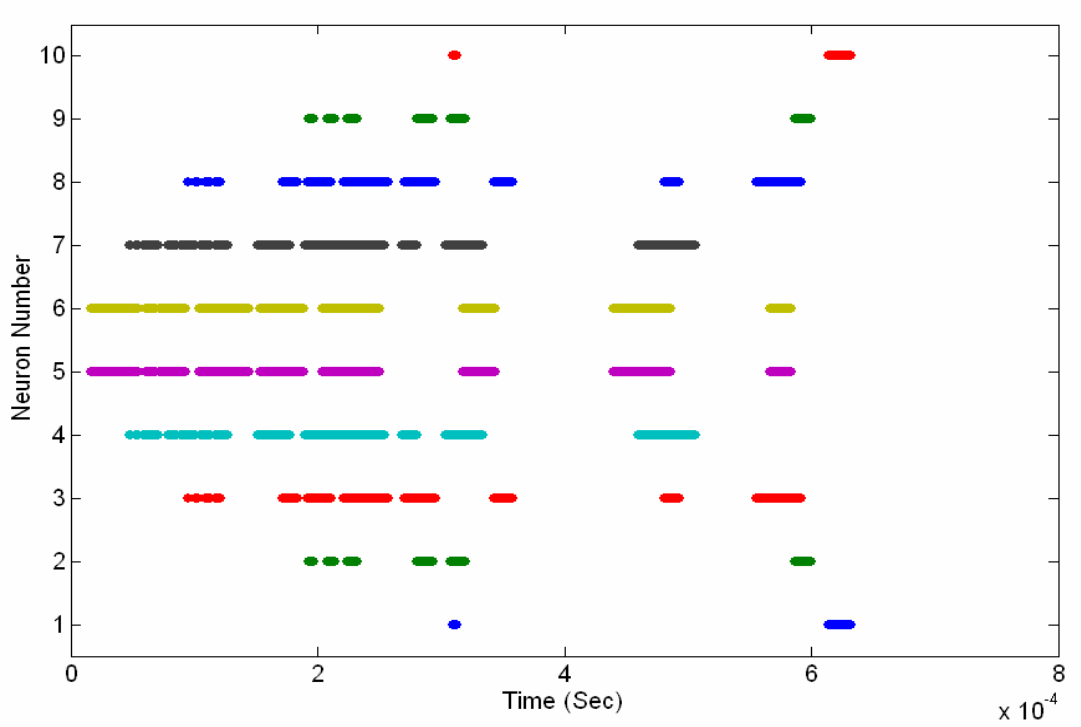

Figure 2.4. Firing of the column (Y) neurons.

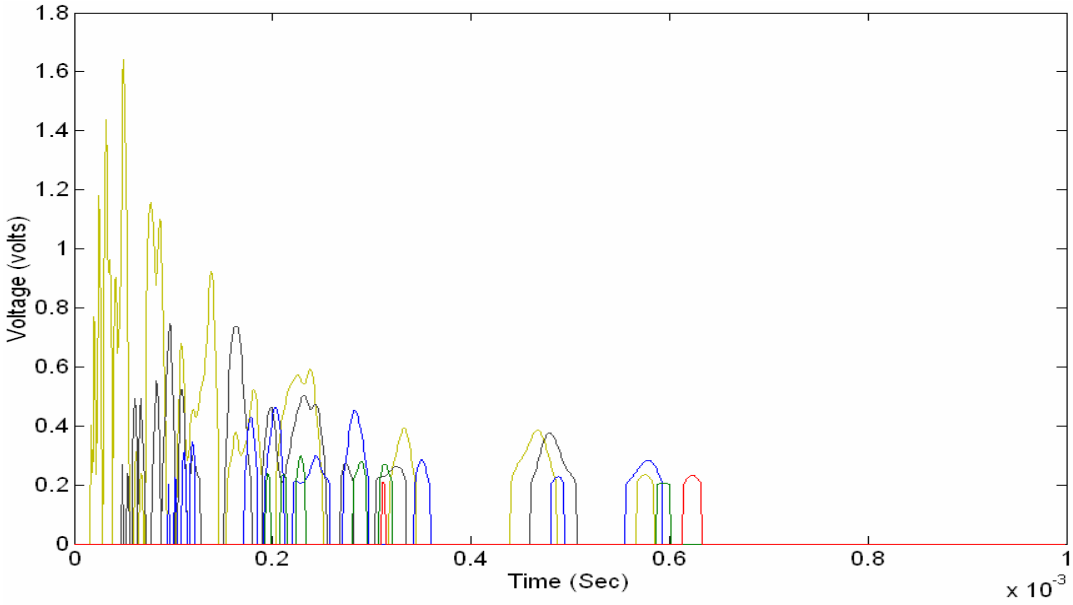

Figure 2.5. Individual responses of the column neurons after firing.

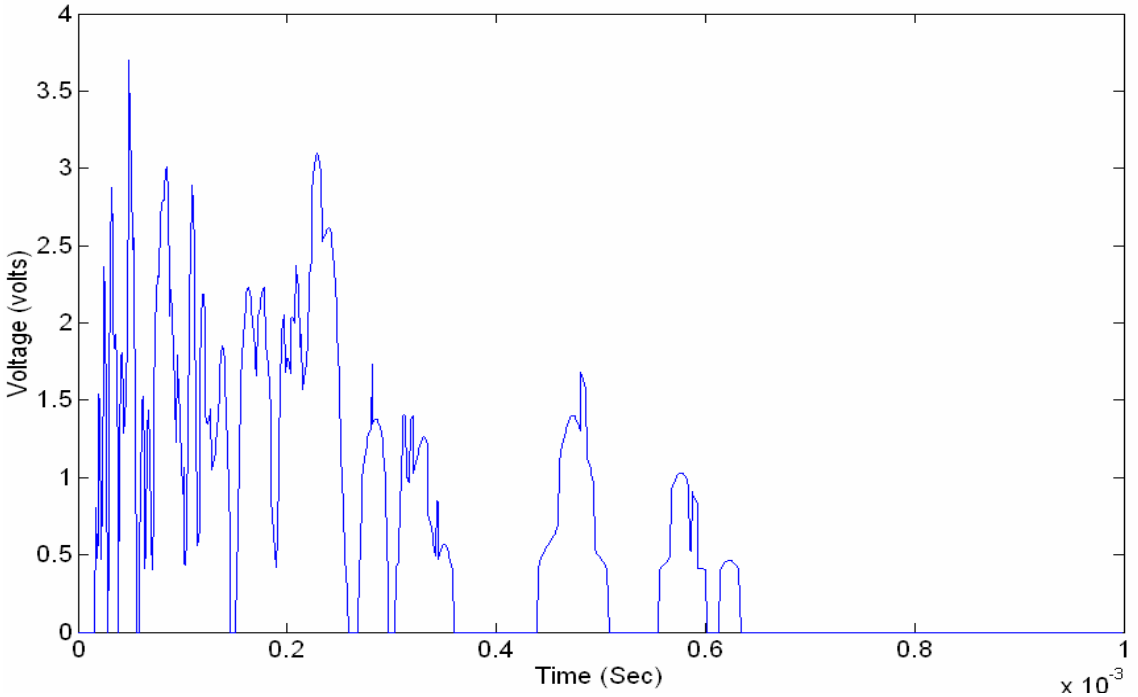

Figure 2.6. Combined output of the column neurons due to an impulse excitation.

There are actually combinations of up to 10 curves in Figure 2.4 and Figure 2.5. The combined row and combined column outputs give a composite response that characterizes the frequency and amplitude level of the excitation. The SNS presented is an efficient method for parallel processing of structural responses and detecting impact and the health of structures. In the response, as the wave propagates, different neurons fire and indicate the location of the damage. The combined output signal shows the approximate amplitude and frequency content of the AE signal caused by the damage. The electronics hardware to achieve a signal processing system similar to that represented in the simulations can be formed using an array of neurons in which each neuron has its own Transducer Bus Interface Module (TBIM). The TBIM and emulator architecture is described later. An approach to reduce the number of TBIMs needed or to further simplify the signal processing architecture needed to process the array data has also been developed. This new architecture is called the SNS. The concept for the SNS was submitted as an invention disclosure at the University of Cincinnati in collaboration with North Carolina A&T State University in 2003.

3.0 Manufacturing and Testing the Structural Neural System

Damage in fiber composite materials is difficult to detect and the use of composite materials is limited by the lack of methods to monitor the condition of structures. There is an increasing need for health monitoring techniques that will allow composite materials to be more widely used. Wind turbine applications are particularly demanding because they require high-reliability and low-cost composite materials. SHM has not been widely used in industry due to the weight, cost, and complexity of the added sensors. In order to detect damage, a large number of conventional sensors and data acquisition instruments must be used to detect damage. Alternatively, an SNS can be formed using a large number of sensor nodes and as few as four channels of data acquisition. This system is configured by a series of continuous sensors connected to a data acquisition computer. The continuous sensors are formed by individual PZT sensors connected in a series. The density of the sensor nodes determines how sensitive the SNS is to detecting minute damage.

This section discusses the fabrication and testing of continuous active fiber composite (AFC) sensors [2, 3, 4] for use in predicting failures in composite materials. Continuous sensors are series-connected sensors, also called neurons, used to form the SNS. This sensor technology has proven to be effective in detecting small damage in structures, such as breaking of composite fibers and delamination. SHM of wind turbines is a potential application of continuous sensors because of the large size of the structure. In order to detect the position of a failure in structures, unidirectional active fiber sensors built from PZT ribbons are considered here. To manufacture the unidirectional sensors, a mold was developed to produce thin composites of aligned PZT ribbons. The sensors produced were tested for their ability to detect AEs. The sensors were bonded to fiberglass plates and, using pencil lead breaks to simulate AEs in the material, limited testing was done cycling the plate in a hydraulic mechanical testing machine to produce damage. The results of these experiments are summarized in this section.

3.1 Fabrication of Active Fiber Continuous Sensors

The procedure developed to fabricate Active Fiber Continuous Sensors (AFCS) is discussed in the following steps (S1 through S6), and in reference [2]. The AFCS is manufactured at the University of Cincinnati in collaboration with North Carolina A&T State University.

(S1). Prepare PZT Ribbon Fibers. The PZT ribbons used for creating the sensors are purchased commercially [5]. These ribbons are PZT 5A fibers with an aspect ratio of 3:1. Since they are brittle, they can easily be cut with a razor blade to the appropriate length for use in the molding process. The manufactured preform and ribbons can be seen in Figure 3.1.

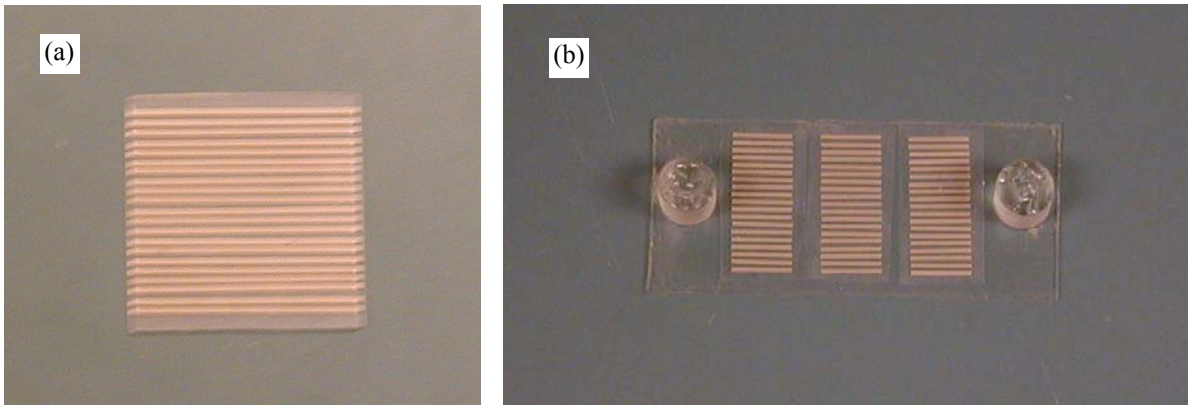

Figure 3.1. PZT actuator preform (a), and acoustic sensor preforms (b).

(S2). Molding. The PZT ribbons need to be placed in an epoxy medium in order to remain at equal spacing and provide strength to the final wafer. To achieve this, two plates were machined out of aluminum and two combs made from key stock were inserted in slots cut in the plate. The combs align the PZT fibers in position so that the EPON Resin 862 epoxy can be injected through one of the top holes. The injector is made from a stainless steel pipe, which is bored out to 5/16 inner diameter, and an aluminum piston, with an o-ring, to force the epoxy out (Figure 3.2). Before being assembled, all pipe connections are sealed with Teflon tape.

Figure 3.2. Piston assembly of the mold for casting the AFCS.

(S3). Assembly. First, starting with the 6½-inch PZT ribbons shown in Figure 3.3 and described above, the ribbons are cut into 3/8-inch pieces using a razor blade. Then, they are cleaned in a bath of acetone and heated for 15 minutes at 200^{o}F so that they will adhere to the epoxy matrix. Next, any part of the mold that comes in contact with the epoxy is coated with a release agent and the fibers are aligned in the combs and attached to double-sided adhesive tape. Then, the three sensor fibers are attached to the top side of the mold, between the injector holes, and the Teflon sheet is placed around them (Figure 3.4). Finally, the bottom plate is bolted on with six, 2-inch x ¼-inch - 20 bolts.

Figure 3.3. Individual PZT ribbons from CeraNova Corporation.

(S4). Casting. To begin casting, approximately 4.25 grams of EPON Resin 862 epoxy is mixed. Next, the hole that the injector is going to be placed into is filled to the bottom of the threads with the epoxy. Then, the injector is filled with epoxy and the base of the injector is screwed on. After this, the screw is tightened down to remove air from the injector and it is screwed into the hole that was previously filled with epoxy. The screw is then tightened until epoxy can be seen filling the opposite hole. This is the point where the plug should be inserted and the spring stiffness (k=45.55 pounds per inch [lb/in]) should be placed in the injector cylinder. After that, the injector's screw should be turned 13 full times in order to create a pressure of about 350 pounds per square inch (psi). The assembled mold is shown in Figure

3.5 along with an updated design of the mold. Finally, the entire apparatus is set in an oven (Fig. 3.5) at 200°F for 2 hours. The curing process is shown below as a plot of temperature vs. time (Figure 3.6). After cooling, the thin wafer of PZT ribbons can be removed from the mold by knocking out the holes or cutting off the ends just inside the injection holes. Each wafer produces three 1-inch x ½-inch sensors.

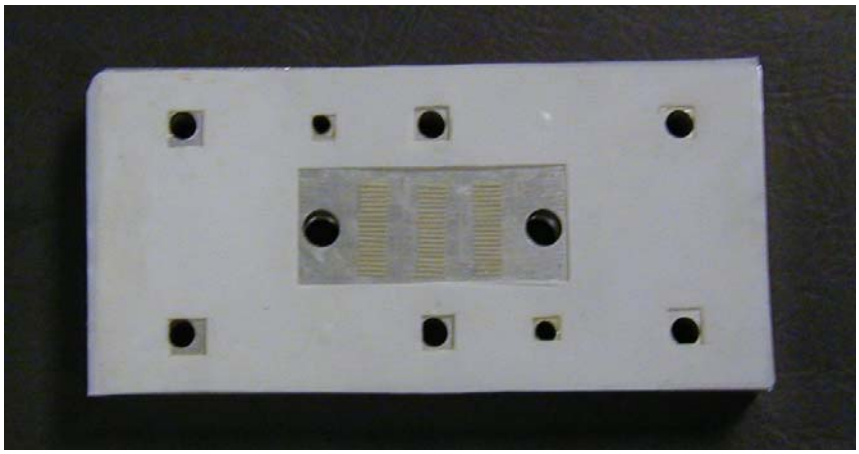

Figure 3.4. Teflon mold and three sensors.

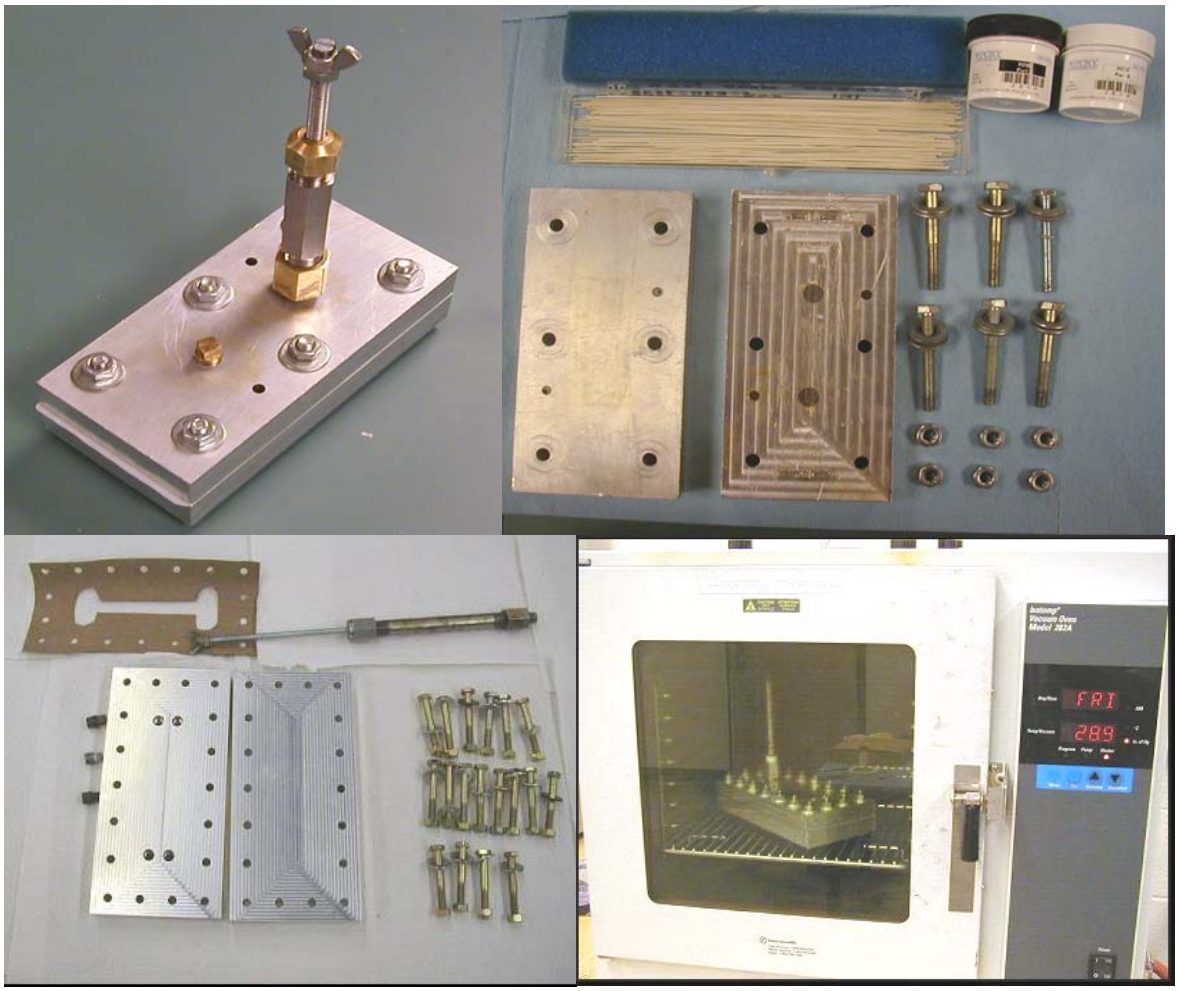

Figure 3.5. Mold for casting AFCS showing original and updated design and curing in an oven.

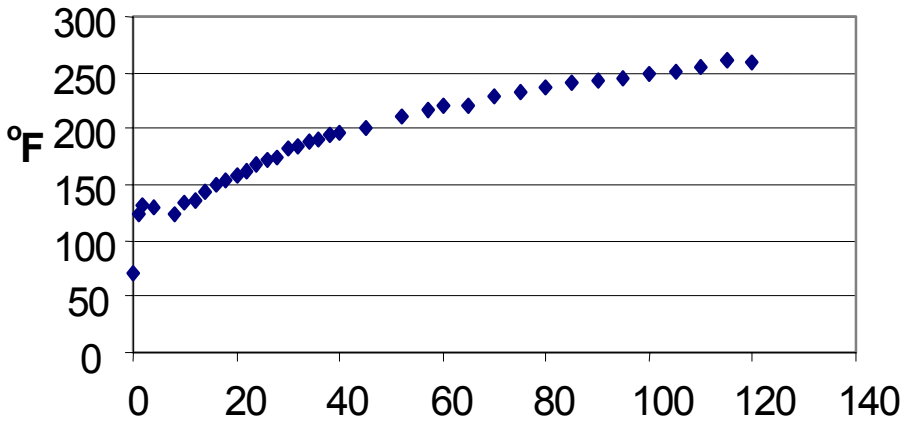

Figure 3.6. Curing process for the AFCS.

The new aluminum pressure mold in Figure 3.5 is being used to manufacture the AFCS. This mold consists of two parts, Part A and Part B. Care is taken while manufacturing the mold so that the tolerance on flatness is maintained at 10 microns. A total of 18 bolts are used to assemble the two parts, which help in reducing the gasket thickness and to allow pressurization to improve fiber wetting. The first mold with the Teflon gasket did not hold high pressure.

(S5). Poling. The fibers in the preform are in the unpoled state and they need to be poled to obtain electro-mechanical coupling. The extent of poling is a function of time, temperature, and the applied field. The bulk coercive field for the PZT 5A material is approximately 11 kilovolts per centimeter (kV/cm). This value was used to determine that 700 volts required for poling the sensors. Poling was achieved by applying the poling voltage at 200°F for approximately 20 minutes. The elevated temperature helps to align the dipoles in the presence of the strong electric field. The voltage is removed after the AFCS has cooled to room temperature. A sensor strip of dimension ½-inch x 1-inch is cut from the preform and sanded carefully until the fibers are exposed. Then the sensor is temporarily electroded on both faces by carefully aligning the copper strips of foil to avoid electric short circuiting. A fixture is made from Teflon plates for clamping the specimen in place and providing the electrical connection. The experimental setup is shown in Figure 3.7.

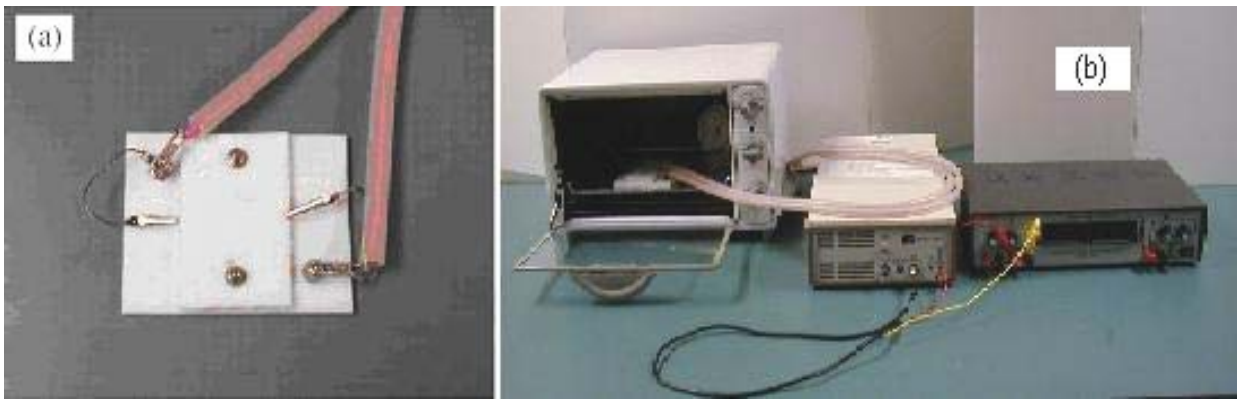

Figure 3.7. Poling setup showing (a) the fixture with high voltage wires and (b) the oven, charge amplifier, voltage source, and fixture.

(S6). Electroding and Assembly. Fabricating the continuous sensors (Figure 3.8) is done by first electroding both sides of a polarized sensor with conductive silver H2OE EPO-TEK epoxy with a strip of copper tape protruding, so that it can be attached to the male connector. The silver epoxy is allowed to cure in the oven between sides. Next, two strips of heat-curing adhesive Kapton are cut, to cover the sensors, and thin ribbons of copper tape deposited on one. Then, other sensors are electroded as before and connected in a series with the first one. After that, the top sheet of Kapton is placed over the entire network and it is placed in an oven at 200^{o}F for 90 minutes. The next step is to solder the copper tape, at the end of the sensor, into pins and insert them into the connector housing. The Kapton can then be cut to shape around the sensor. Figure 3.8 is an individual node with silver deposited on it and when attached in a series it forms the continuous sensor. This forms a neuron that functions much like the neuron in the human body's nervous system. A single- and a two-node sensor are shown in Figure 3.9.

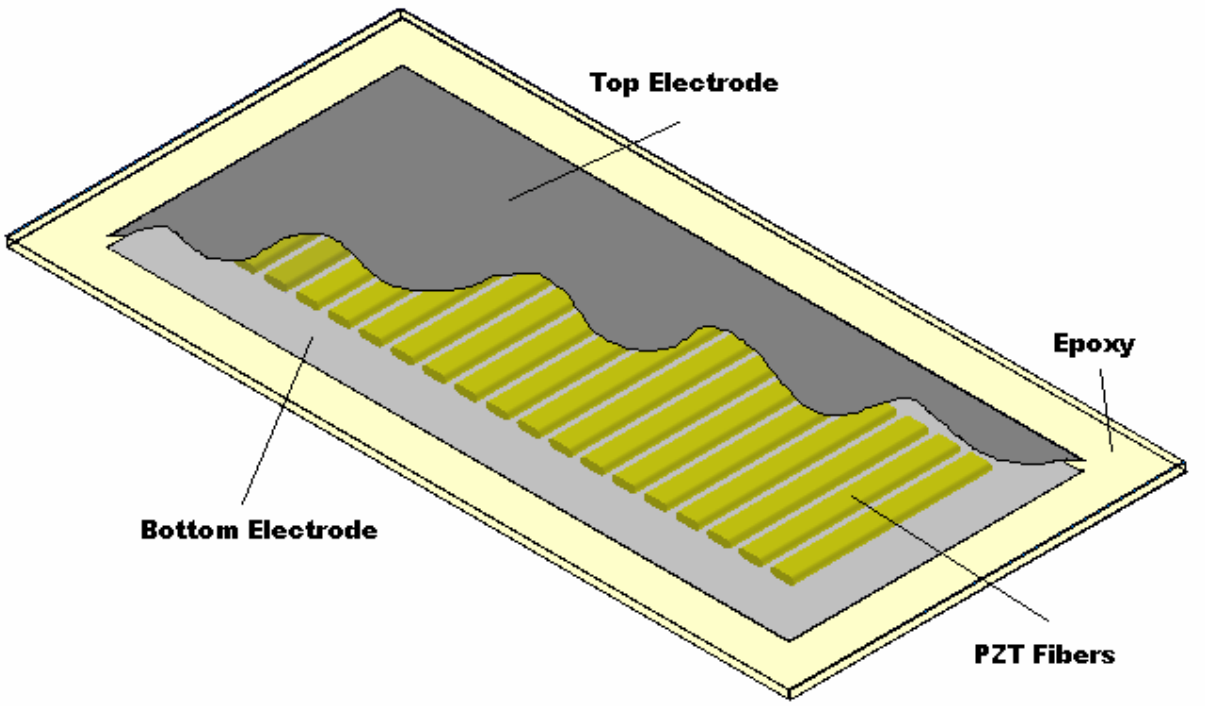

Figure 3.8. Sketch of the components of the AFS.

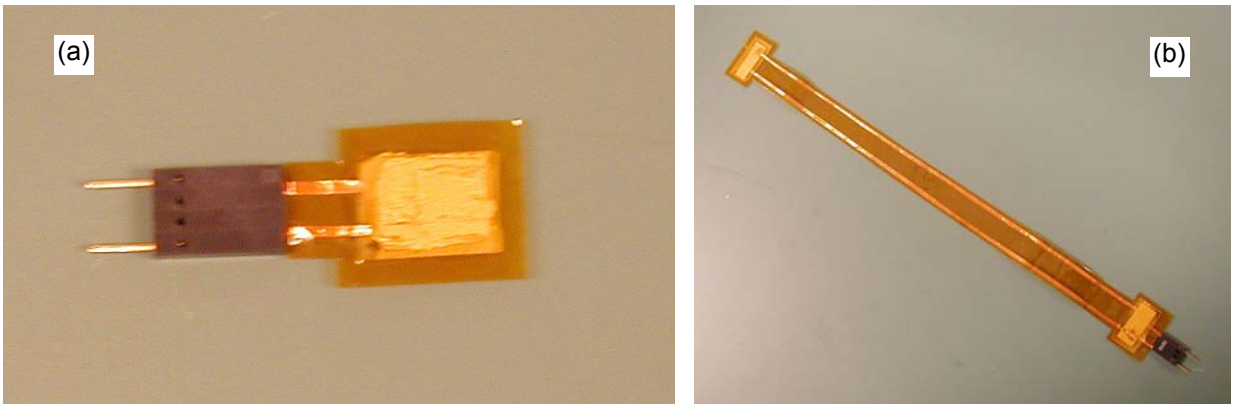

Figure 3.9. The active fiber sensor; (a) an individual sensor and electrodes, and (b) a continuous sensor with two nodes. The sensing direction is along the length of the sensor.

3.2 Modeling of Piezoceramics

To relate mechanical and electrical fields, the piezoelectric constitutive equation is used as:

$$\begin{bmatrix} D \\ S \end{bmatrix} = \begin{bmatrix} \varepsilon^T & d \\ d_t & s^E \end{bmatrix} \begin{bmatrix} E \\ T \end{bmatrix} \tag{1}$$

The Equation (1) is a coupled field equation that relates the applied electric field $(E)_{3x1}$ in kV/cm, the electric displacement $(D)_{3x1}$ in coulombs/m^2, the strain $(S)_{6x1}$, and the stress $(T)_{6x1}$ in (MPa). Material properties such as the dielectric permittivity $(\varepsilon^T)_{3x3}$, the induced strain $(d)_{3x6}$, and the compliance $(s^E)_{6x6}$ are used to relate the mechanical and electrical fields. The subscript t means transposed. The superscript T represents a constant stress condition, often taken as the unclamped or free mechanical boundary conditions. The superscript E represents a constant electric field condition, which is satisfied with short-circuited electrodes. With the assumption that vibration occurs only in the X-direction and the AFS is poled in the Z-direction and using other relations, Equation 1 reduces to:

$$D_3 = e_{31} S_1 + \varepsilon_{33}^S E_3 . \tag{2}$$

Solving for the current:

$$i = \dot{Q} = \dot{D}_3 A_e \tag{3}$$

where Q is the charge on the electrodes, and A_e is the electrode area of the PZT wafer. Substituting Equation (2) into Equation (3) gives:

$$i = e_{31} A_e \dot{S}_1 + \varepsilon_{33}^S A_e \dot{E}_3 . \tag{4}$$

The permittivity at constant strain is:

$$\varepsilon_{33}^S = \frac{C_p h_e}{A_e} \tag{5}$$

where C_p is the capacitance, h_e is the electrode spacing, and A_e is the electrode area of the PZT. Substituting Equation (5) into Equation (4) gives:

$$i = e_{31} A_e \dot{S}_1 + C_p h_e \dot{E}_3 . \tag{6}$$

The voltage field is:

$$E_3 = V / h_e . \tag{7}$$

Substituting Equation (7) into Equation (6) gives:

$$i = e_{31} A_e \dot{S}_1 + C_p \dot{V} . \tag{8}$$

This shows that the current is proportional to the strain rate and to the rate of change of the voltage across the PZT. The PZT material in an electrical circuit acts like a capacitor in which electrons collect on the electrode plates but do not flow through the dielectric material. Strain causes a change in attraction across the PZT, and electrons collect on the electrodes in proportion to the strain rate of the PZT. If $i = 0$, which simulates an open circuit when voltage measurements are made, then:

$$V = \frac{e_{31} A_e}{C_p} S_1 + V_0 . \tag{9}$$

The last equation relates the voltage generated in an open circuit by the AFS under dynamic strain conditions. In this equation, A_e is the area of the electrode, V_o is the initial voltage, e_{31} is the induced stress constant, and C_p is the capacitance of the AFS sensor. Equation 3 can be used to find the d_{31} coefficient by knowing the load and the loading cycle of the mechanical test machine. The voltage produced can be monitored by an oscilloscope. Full details of the modeling are given in reference [1]. Other references that give information on piezoelectric sensors are [6−14]. This modeling is used in the wave propagation simulation algorithm to study sensor designs. The experiments performed to test the continuous sensor are described next.

3.3 Individual Sensor Testing

In order to show unidirectionality of the sensors, this experiment involved two sensors bonded to a ¼-inch fiberglass sheet where the sensors were perpendicular to each other and independently connected to an oscilloscope to record the responses. This setup is shown in Figure 3.10. A 0.7-millimeter (mm) pencil lead was broken at the designated point. The lead break acts similarly to a fiber failure in the fiberglass plate. Figure 3.11 shows that the sensors are more sensitive to longitudinal waves than transverse waves. This is shown by the higher voltage of the longitudinal sensor. The reason for this is that the PZT ribbons are bonded in the epoxy matrix in such a way that they become strained more in the longitudinal direction than in the transverse direction. This causes a larger charge difference on the longitudinal sensor.

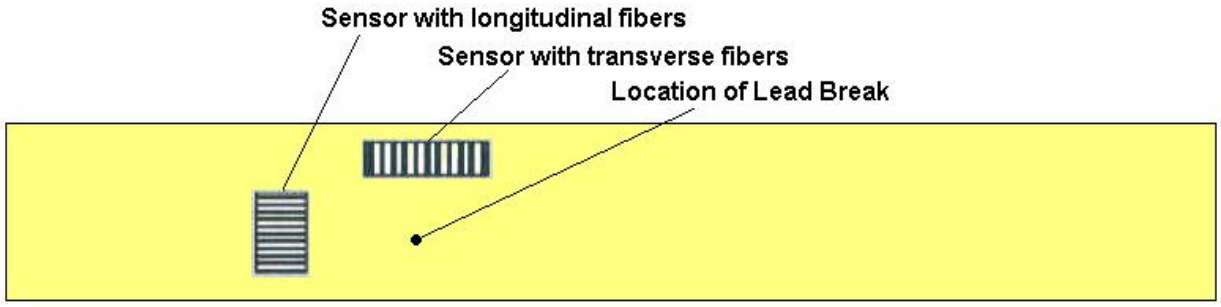

Figure 3.10. Sensors on a long fiberglass panel to simulate a wind turbine blade.

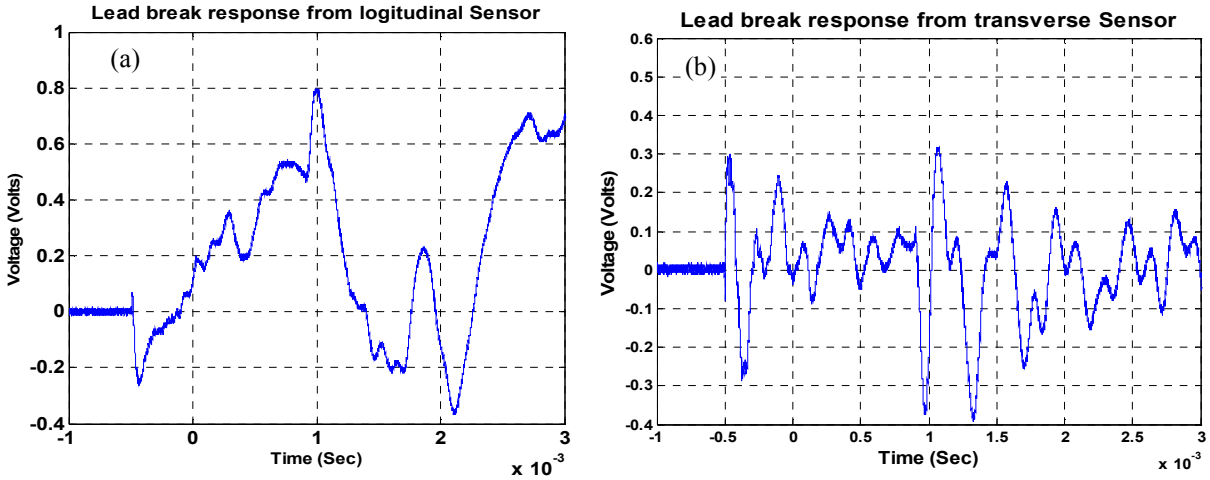

Figure 3.11. Responses of the longitudinal (a) and transverse (b) sensors.

3.4 Fatigue Monitoring of a Composite Bar

A fatigue test in a mechanical test machine is described next. For this test, one sensor was bonded to the surface of a ¼-inch composite fiberglass sheet. It was then cycled in an MTS machine at 2 Hz until failure. Figure 3.12 shows the received AE from initial crack propagation in the composite. This is a high-frequency signal that can be seen decaying over time. In Figure 3.13, the signal is the final failure AE. This is the point where the crack propagates very quickly and splits the composite board into two pieces. The left plot is the unfiltered signal and the right plot is the same signal but passed through a high-pass filter. This shows the very high-frequency AE produced at total failure.

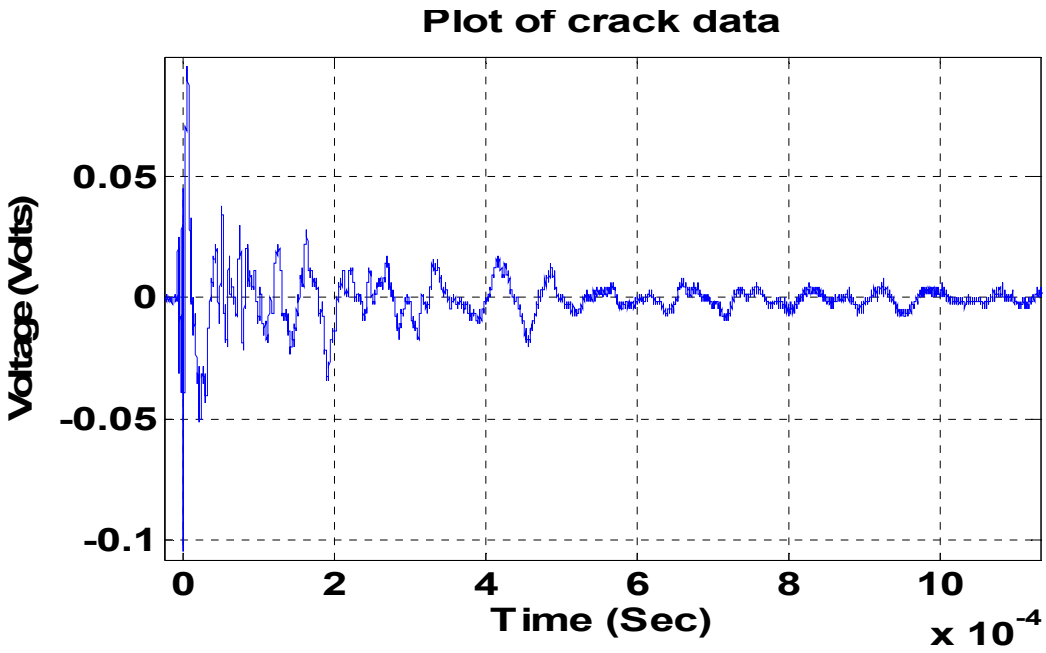

Figure 3.12. AE due to initial crack propagation.

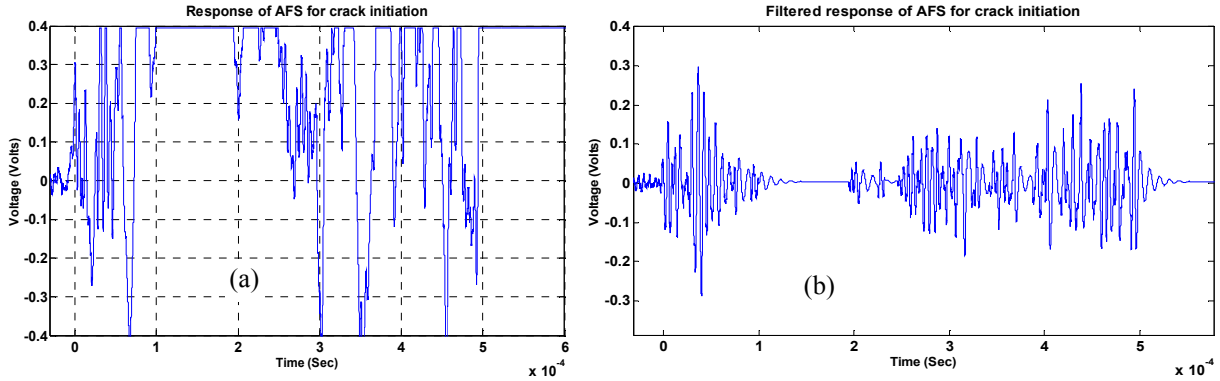

Figure 3.13. Unfiltered (a) and filtered (b) signals at final failure.

The signals at final failure are important because they show the sensor did not fail due to the high strains and the sensor was able to record the very high signal level. The AE that was caused by initial damage was detected and would therefore warn of damage so that the wind turbine could be stopped to prevent failure, as occurred in Figure 3.13.

3.5 Testing the Continuous Sensor

For this experiment the two individual active fiber sensors were bonded to a fiberglass plate with length 0.5 m, width 0.08 m, and thickness 0.003 m. Node 1 is at 0.14 m from the left edge and node 2 is at 0.34 m from the same edge. Each sensor node is 0.0127 m long, 0.0254 m wide, and 0.00034 m thick and contains 21 ribbon fibers. When connected together in series this produces a continuous sensor as shown in Figure 3.14. The resistance and capacitance of the sensor are checked at the beginning and end of the testing to verify the sensor properties. All of the plots were produced by breaking a 0.7-mm lead pencil on the edge of the plate to produce a longitudinal wave. The lead break is a good simulation of an actual

fiber break. The sensor response to the lead break is checked at the beginning and end of the testing to verify that the sensor is bonded properly to the panel.

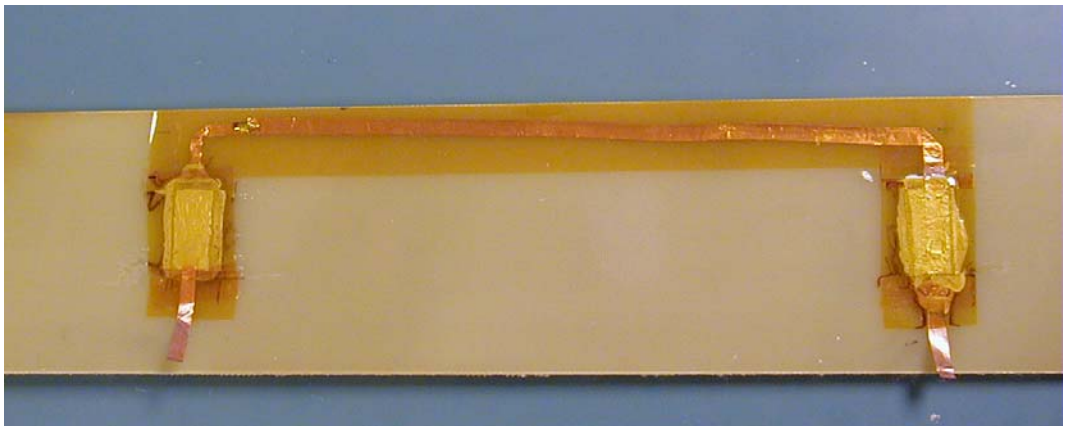

Figure 3.14. Series-continuous sensor on a fiberglass plate.

The experimental setup for testing the active fiber sensors is shown in Figure 3.15. The fiberglass beam with the mounted sensors is cycled in three-point bending and the signals from the sensor are filtered and then recorded on a digital oscilloscope.

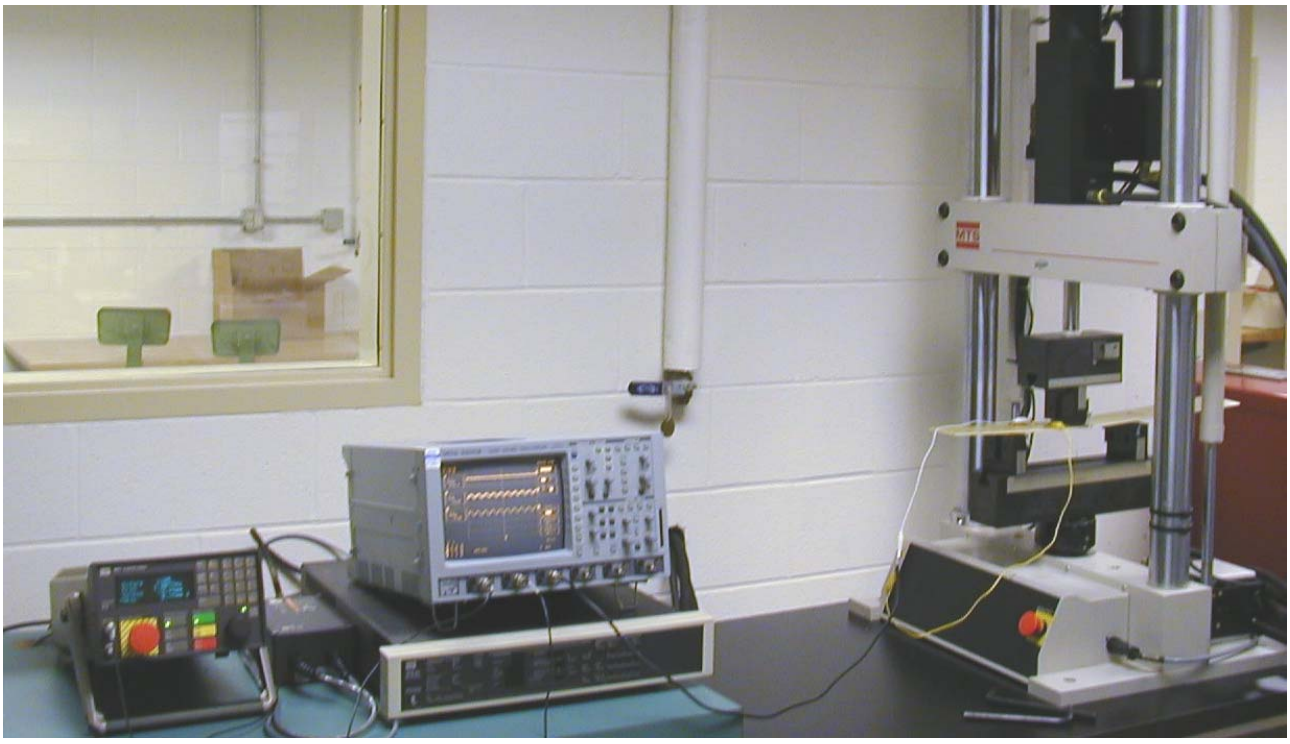

Figure 3.15. Experimental setup for testing of continuous sensors bonded on a structure.

For the first part of the experiment, the sensors are disconnected from being in a series and connected to individual channels of the oscilloscope. In Figure 3.16 it can be seen that sensor 1, closest to the AE, records the signal before sensor 2, the farther one. The time difference between the two recorded signals was about 53 microseconds. By knowing the time difference and the 0.20-m spacing between the nodes,

we can find the velocity of the wave, which is then used to find the elastic modulus of the fiberglass plate. If the modulus changes, this is another way to indicate damage.

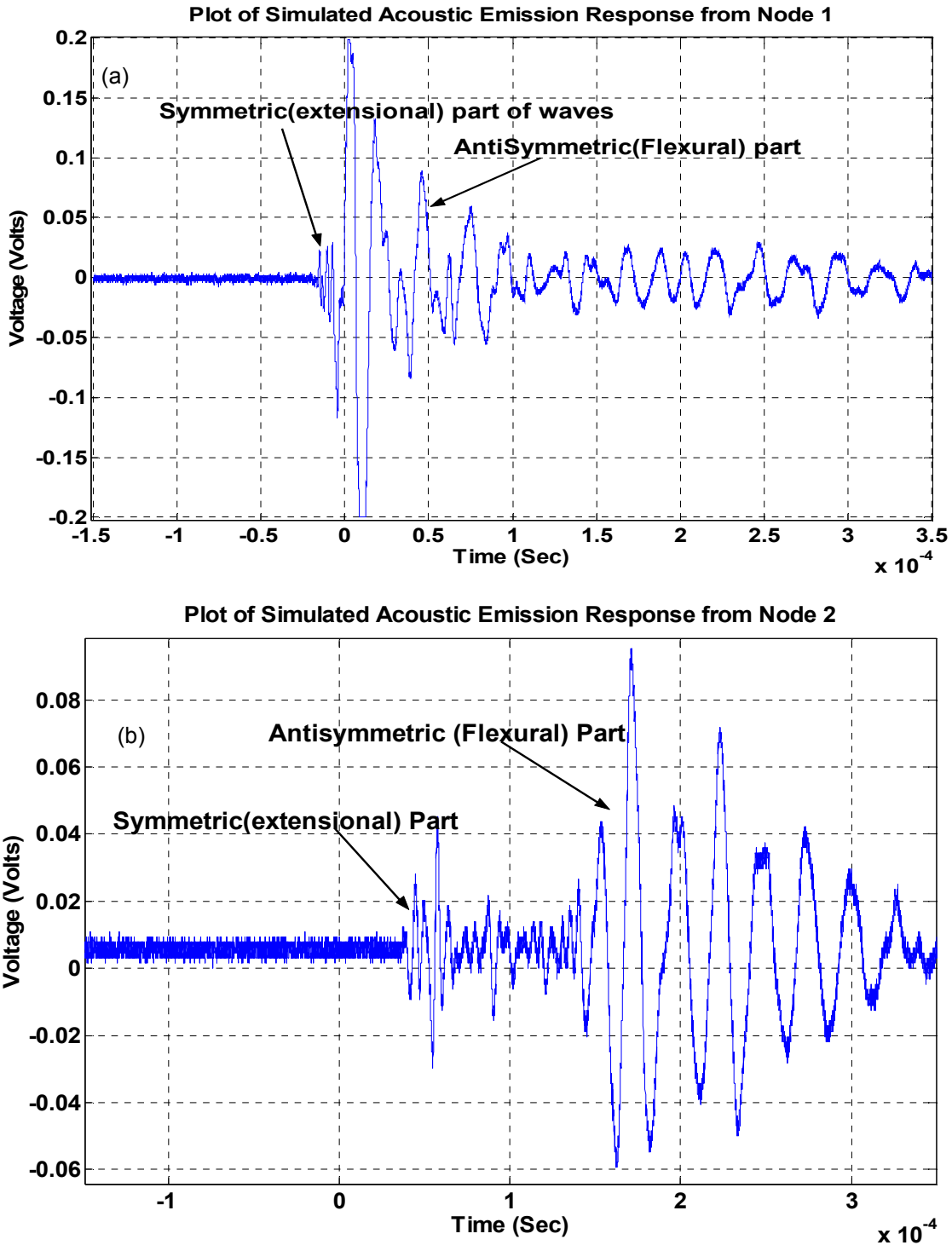

Figure 3.16. AE at individual sensors; (a) at sensor 1, and (b) at sensor 2.

For the second part of the experiment, the two sensors are reconnected in a series and a similar lead break was performed. In Figure 3.17, the different wave components can be identified as the wave travels some

distance. This is used to determine the required spacing of the sensors and to set the filtering frequency of the signal processing unit. A multiple-node continuous sensor is used as a neuron in the neural system and the response is used to identify and locate damage in the SNS.

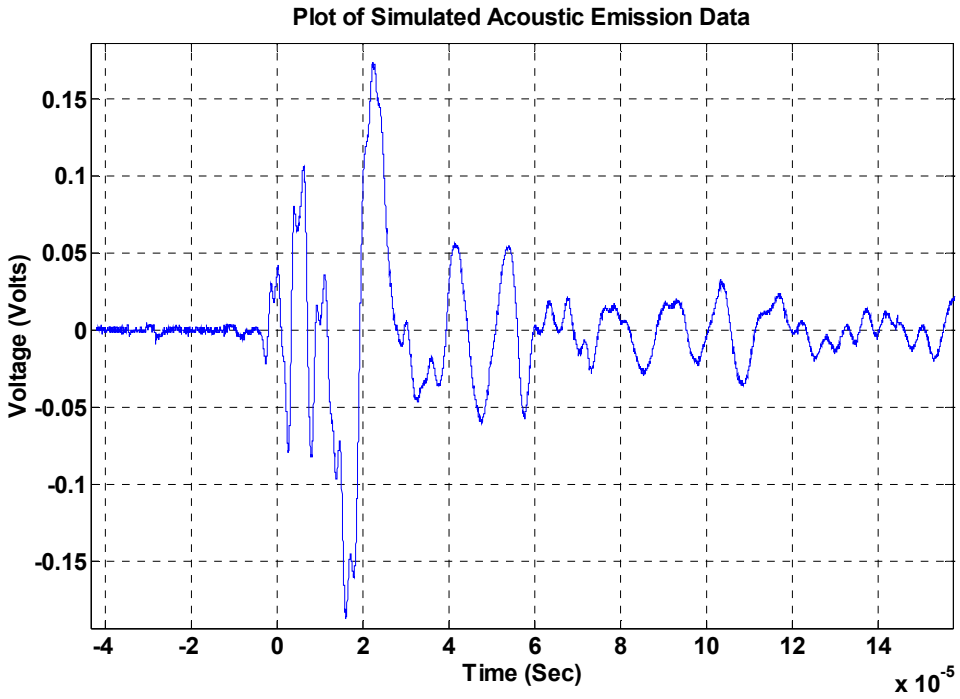

Figure 3.17. Response of the two-node continuous sensor.

Continuous sensors using PZT ribbons can detect minute AEs in structures. The advantages of the continuous sensor compared to other sensors are that it can have many closely spaced sensor nodes and thus becomes more sensitive, it may be used in complex geometries, and can be placed close to the damage. The PZT can be molded to different shapes depending on the application. The rectangular ribbon fibers in the epoxy make the sensor rugged and conformable. The methods we have developed allow creation of flat planar sensors, which detect damage along plates and shell structures. The silver epoxy is used to bond directly to the fiber/epoxy sensor surface and to the structure or the Kapton, and a silver epoxy lead is used to connect to the copper foil electrodes. This provides improved strain transfer and increases sensor voltage.

The responses received from the AFS were reproducible and had a good signal-to-noise ratio. Continuous sensors allow the damage location to be determined by filtering and using a computer with only one channel of data acquisition. The fibers make the sensor mostly a unidirectional sensor, which is advantageous in locating AEs in some circumstances. An important result of testing the AFC sensor was to show that possible shear lag and the very narrow sensor (two fibers wide) reduced the low-frequency components of the signals. Testing the Active Fiber Continuous Sensor in a fatigue test of a beam showed the sensor has good sensitivity and is rugged. AEs were detected when a seeded crack began to propagate. The frequency of occurrences and the amplitude of the emissions increased up to failure of the fiberglass bar. An array sensor system with two rows and two columns was also built and tested on a composite panel (results are not shown). This testing used four channels of data acquisition and the computer was used to represent the functions of the neural system, including firing the neurons. This array sensor was able to detect simulated AEs using a lead break anywhere in the panel.

3.6 The Structural Neural System Processor

The previous work produced an active fiber-composite design of the continuous sensor. The continuous sensor can also be formed by connecting monolithic wafers in series. The next step was to develop the signal processing architecture of the SNS by mimicking the biological neural system using electronic logic circuits. The biomimetic SNS was developed to provide health monitoring capability using a passive-signal processing architecture and continuous sensors. A two-neuron SNS was constructed first. Testing the functions of the neural system including firing of the neurons was done and the two-sensor system was able to detect simulated AEs using a lead break, and it identified which neuron the signal was coming from. The next step was to expand to a four-neuron system. Details of the design and testing of the SNS processors are given in references [16−21]. The neural system processor includes charge amplifiers, comparators, an active filter, and other components. Since the charge produced by an AE sensor is very small, the amplifier electronics are needed to amplify the output voltage of the sensor. A charge amplifier is used that amplifies the voltage output based on the feedback capacitance (C2) shown in Figure 3.18. The output of this circuit is represented by V=Q/C2. This equation proves that the output voltage is dependent on the feedback capacitance C2 and not on the sensor's capacitance (C1) or the cable capacitance (not shown in the circuit diagram). The OPA627 op-amp shown in Figure 3.18 was obtained from Texas Instruments and is used in the SNS processor circuit. This op-amp has a low input bias current and is used typically for piezoelectric sensor applications.

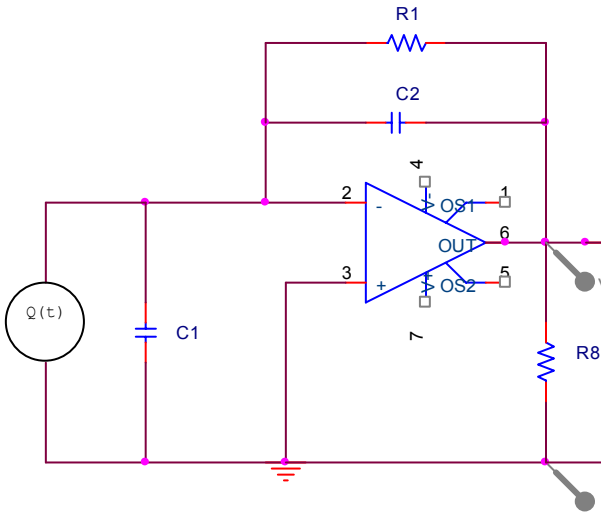

Figure 3.18. Charge amplifier circuit.

The output of the charge amplifier is sent to an active filter to reduce the unwanted low frequencies in the circuit. Figure 3.19 shows the combined circuit involving both the charge amplifier and the active filter circuit that is the front end of the electronic neuron that mimics the signal processing in the biological neuron. The TL071CP op-amps were used for active filter circuit. Input bias current for the active filter circuit is typically between 60 and 200 picoamperes. The output impedance of the charge amplifier is very small and hence a high current exists at the output of the charge amplifier. The TL071CP can therefore be used as opposed to OPA627, which has been used for the charge amplifier circuit. The filtering design is an important part of the SNS for AE sensing. Filter bandwidth and gain should be adjusted for specific types of structures and materials [19]. Design of the control panel for the SNS was done using LABVIEW and is described in reference [22]. Processing the acquired data using LABVIEW was done using MATLAB software.

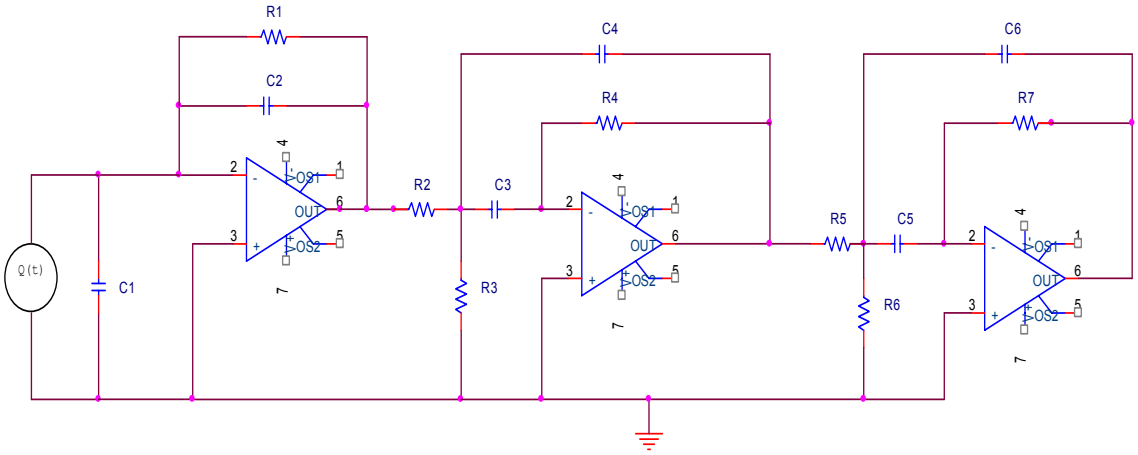

Figure 3.19. Combined circuit involving both the charge amplifier and the active filter circuit.

3.7 Fatigue Testing

A two-neuron SNS using aluminum beam specimens with PZT monolithic sensors was tested (see Figure 3.20 and Figure 3.21). Aluminum is used here to test the sensitivity of the SNS.

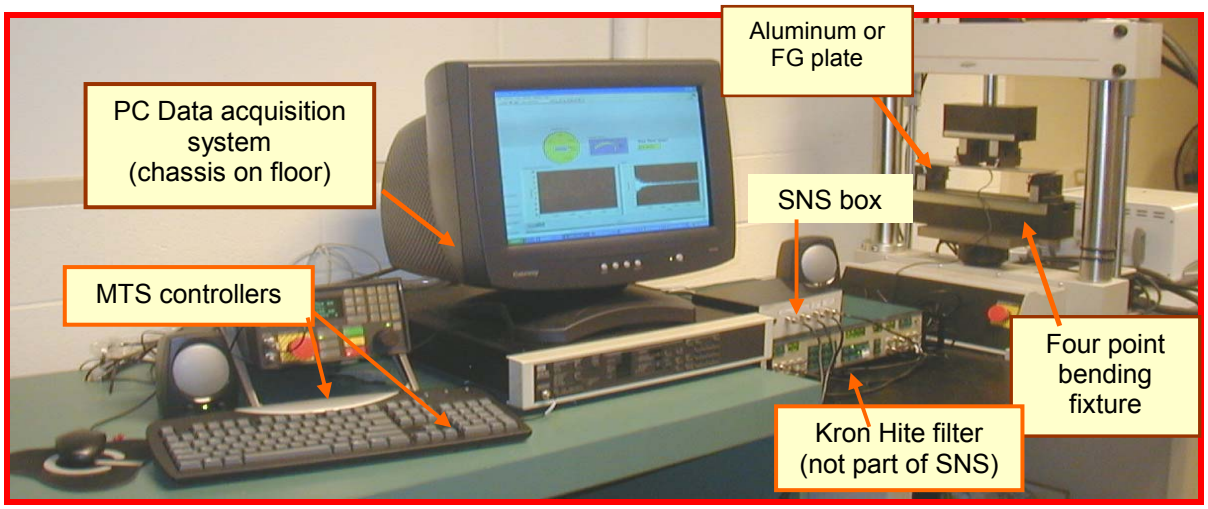

Figure 3.20. The SNS capturing data in a fatigue test. Only the PC and SNS box are used.

Figure 3.21. Beam with a fatigue crack monitored by two single node neurons. The raw AE signal is shown. In larger structures, the neurons will be continuous fibers.

This testing showed that the AE signal level is much lower in aluminum than in composites. When the sensor is close to the crack, the AE level is detectable. A Damage Modeling and Prognostics Method is being developed to equate AE data to damage. See equations 1-2:

$$2a = \frac{C_E}{\frac{dC_E}{d(2a)}} + 2a_0; \quad 2a = \frac{C_A}{\frac{dC_A}{d(2a)}} + 2a_0; \quad (2a - 2a_o) \geq 0 \tag{1, 2}$$

where C_E, C_A, a are the cumulative AE events, the cumulative AE amplitudes from the sensors, and the predicted crack length, respectively. The use of damage prognostics with the biomimetic SNS is just being developed and should be verified by experimentation on different types of structures. Some initial work was done testing an aluminum joint using a two-neuron SNS. There will be joints in the wind turbine where fatigue can occur. (There is very little information in the literature on health monitoring of joints.) It was found that the AE level is much lower in the aluminum joint than in the fiberglass used in our typical testing. This indicates the need for a long continuous sensor to be close to any possible damage site.

3.8 Development of Carbon Nanotube Neurons

A novel idea for a new type of continuous sensor was tested in a preliminary way in this project. A carbon nanotube (CNT) film (buckypaper) was produced by solution casting CNTs dispersed in a solvent and bonding the film onto a small aluminum beam. A fine crack was developed in a beam and the beam was cycled to propagate the crack. The nanotube film sensor produced a sinusoidal signal based on the piezoresistive property in which the resistance changes with strain. When the fine crack passed through the film sensor the electrical circuit became open and the sensor signal became zero. This is a very simple state sensor (on/off) that might be useful in SHM of components with high-feature density where wave propagation is difficult. The SNS is a generic sensor system architecture and different types of sensors, including the piezoresistive sensors, can be used. The buckypaper film sensors have some disadvantages. The film is brittle and difficult to apply on large structures. Therefore, we developed a new method to form the sensor.

The general CNT neuron sensor is basically a long continuous-strain sensor that can be used in the SNS. The SNS can use multiple neurons and can monitor strain (using CNT neurons) or crack propagation (using piezoelectric ribbon neuron) in a structure in real time. The new CNT neuron was fabricated as a long film that was sprayed on the surface of a composite beam to simulate a wind turbine blade. The CNT neuron can be any shape including a grid that is attached onto a structure that functions like the neural system in the human body. The high cost would be a factor for large structures using a single wall carbon nanotube (SWNT) based neuron sensor. Therefore we are investigating building the SNS using multi-wall carbon nanotubes (MWCNT) and carbon nanofibers (CNF) instead of SWCNT. The CNF have lower electrical conductivity than SWCNT, and show less strain sensitivity. The sensing properties of CNF are still being investigated for SHM, but the CNF can reduce the cost in large structural applications such as wind turbines. Figure 3.22a shows a nanotube neuron formed using polymethyl methacrylate (PMMA) and 10 weight percent MWCNT. The neuron is about 15 cm in length. The CNT neuron is actually bonded onto a capton film that in turn is bonded onto the aluminum beam. An epoxy coat is used to cover and protect the neuron. The CNT neuron is connected to a wheatstone bridge circuit and to an amplifier, filter, and an oscilloscope. The setup is very similar to a strain gage measurement system. Figure 3.22b shows the free vibration response of the CNT neuron due to an initial displacement (1 cm) of the free end of the beam. Figure 3.22(c) shows the free vibration response of the CNT neuron due to an impact on the free end of the beam. The response of the beam shows that the neuron can be used as a distributed strain sensor. The CNT neuron might be thought of as many strain gages connected in a series. If there is damage (e.g., high strain due to cracking or delamination) anywhere along the

length and underneath the sensor, the strain will increase and be detectable by the change in electrical resistance. The electrical resistance is the integration of the resistance along the length of the neuron. Thus, a large change in resistance in one local area of the sensor will be detectable. The exact location of the damage along the neuron cannot be determined by the resistance measurement alone. Multiple neurons in a grid pattern or several neurons in a local area can be used to locate the damage.

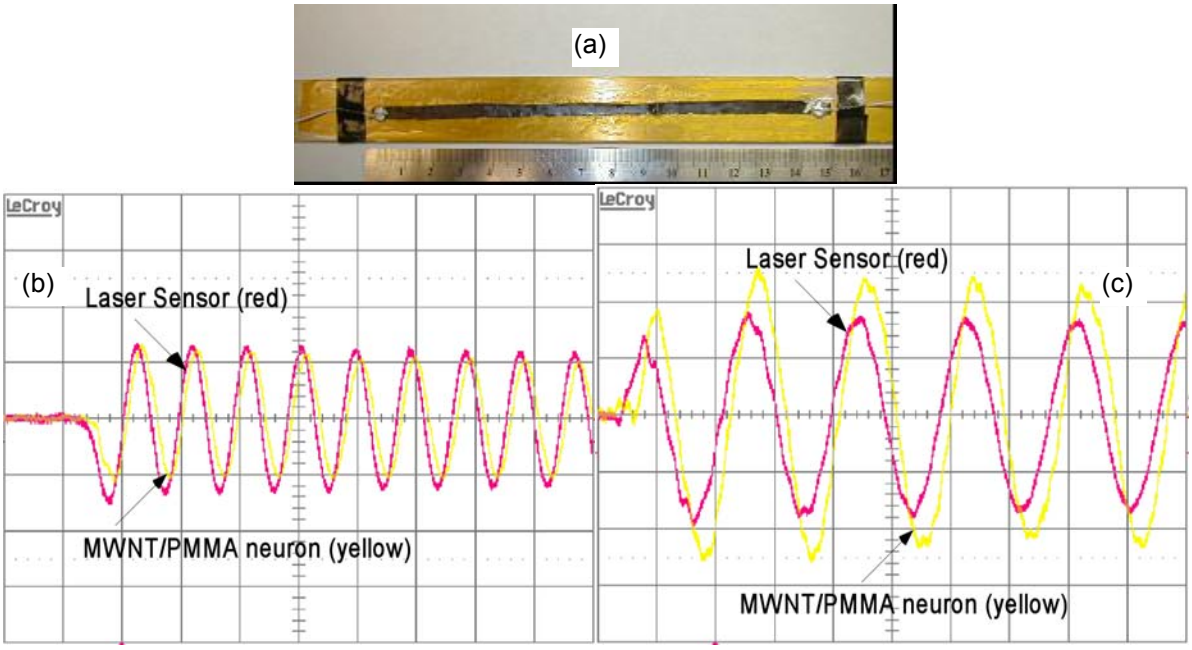

Figure 3.22. The MWNT neuron, continuous strain sensors and its dynamic response in a cantilever: (a) PMMA-MWCNT 10% wt neuron (150 mm x 4 mm x 0.08 mm) on an aluminum bar; (b) free vibration response due to an initial displacement (1 cm) of the free end of the beam; and (c) free vibration response due to an impact on the free end of the beam.

Significant recent progress was made in developing nanotube continuous sensors that mimic biological neurons. Different compositions of carbon nanotubes/nanofibers and polymer were fabricated to tune the sensitivity of the neuron. Also, a spray-on neuron has been initially tried as shown in Figure 3.23. The spray-on neurons may become a great approach for monitoring large structures such as wind turbines.

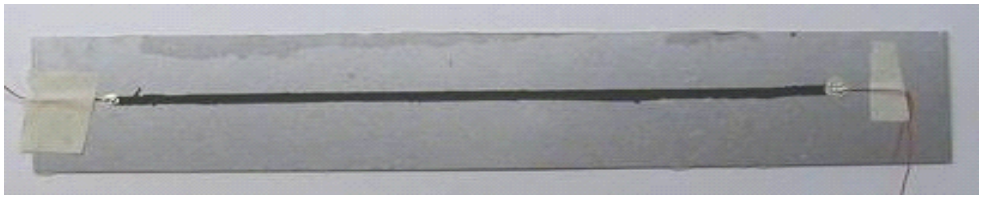

Figure 3.23. The first spray-on piezoresistive CNT neuron on an insulated thin aluminum strip.

Uniform dispersion of the nanotubes to obtain conductivity at the material's percolation level is a problem that we are working on using several approaches. Different compositions of nanotube sensor are shown being tested in Figure 3.24.

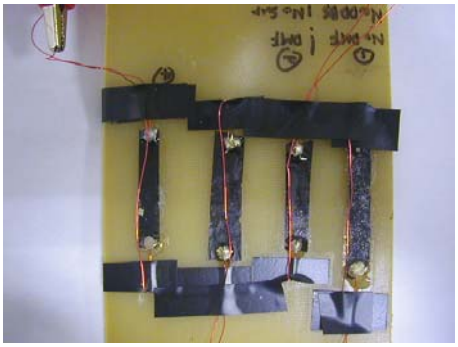

Figure 3.24. CNT polymer sensors on a fiberglass beam simulating a wind turbine blade.

A CNT neuron was sprayed onto a long fiberglass beam simulating a wind turbine blade as shown in Figure 3.25. The resistance of the neuron was high due to the length. Different methods of fabricating the neuron are being investigated. Piezoresistive sensing is used to detect damage using a low-frequency (≈100 Hz) data acquisition system.

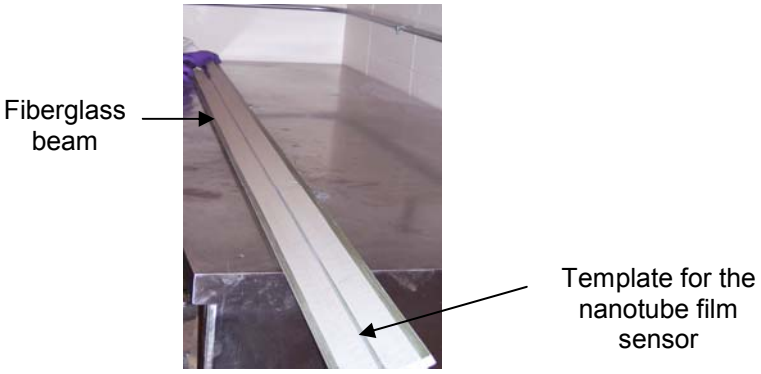

Figure 3.25. A fiberglass beam has been taped and the CNT neuron is being sprayed on.

The piezoresistive sensing property (resistance changes with strain) of CNT composites is used as a sensitive crack and corrosion sensor. Cracking and corrosion can be sensed independently using the same sensor by changes in electrical resistance and capacitance. Strain sensing requires a grid of fine neurons (a sensor film) wherein damage breaks the neuron and opens the circuit. For corrosion monitoring, a 50x change in double-layer capacitance of a neuron occurs at the beginning of corrosion (electrolyte in contact with the neuron). An SHM technique is being developed in which a CNT solution is sprayed onto a structure to form a structural neuron to detect cracking, delamination, and corrosion.

With the recent good results obtained testing the CNT neuron, there appear to be two sensor types that can be used in the SNS, the piezoelectric AE sensor, and the piezoresistive CNT distributed strain sensor. The CNT sensor is simpler but may not have as high sensitivity as the piezoelectric neuron. Also, the signal processing for the neuron will be similar but have different filters and firing levels. Our opinion is that these two sensor types used within the SNS will provide a sensitive, cost effective, and practical approach for SHM of large structures.

3.9 Monitoring a Wind Turbine Blade for Damage during Proof Testing

SHM proof testing of a wind turbine blade was performed at NREL in January 2006. A 12-node four-channel SNS was placed on top of the blade. The SNS detected damage early and multiple damage sites on the blade were identified well before the catastrophic failure of the blade. Strain gages on the blade indicated damage at various locations just before buckling failure. The damage location predictions using the SNS are shown in Figure 3.26 and were approximately verified based on the locations of strain gages. Continuous sensors were also placed on the top and bottom of the blade and signals were recorded independent of the SNS. The continuous sensors were connected to a commercial AE monitoring system. The continuous sensors detected more AEs than the SNS due to the lower settings for signal acquisition. The continuous sensors successfully detected damage early and tracked the AE occurrences during the damage growth. Details of the testing are given in reference [23].

The results of this test demonstrated that the SNS is a viable method for SHM of complex composite structures. We suggest that future work include testing a larger SNS on a wind turbine blade during fatigue testing, and to test the SNS on other components of the wind turbine.

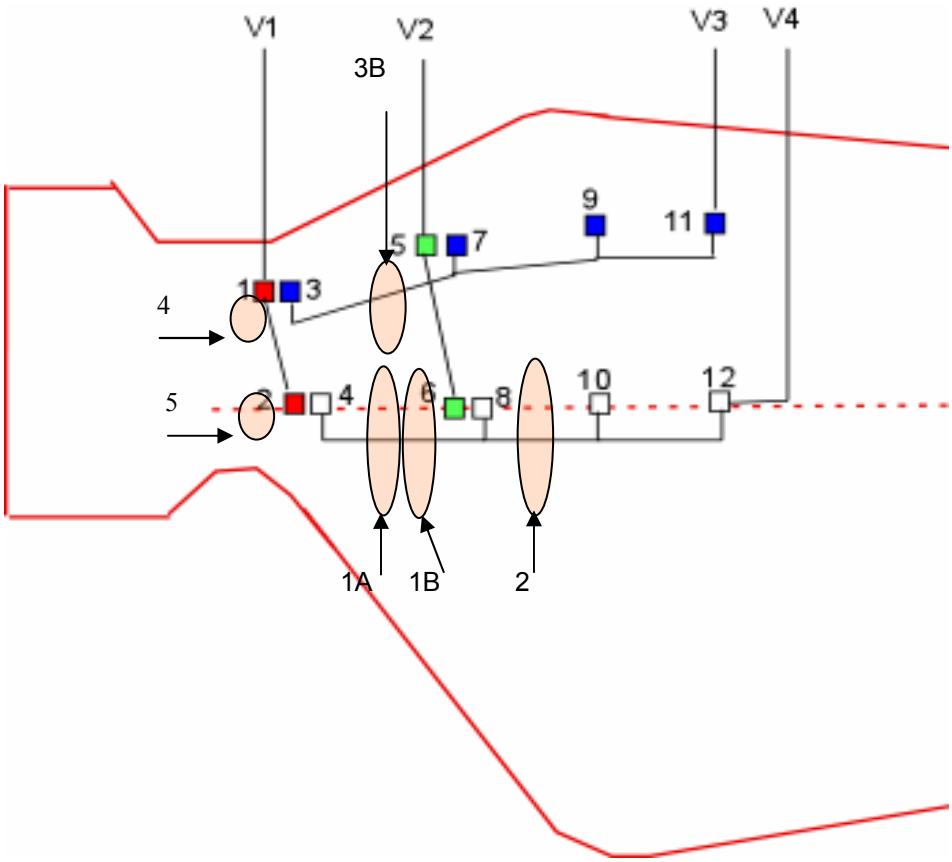

Figure 3.26. Schematic of the SNS on the test wind turbine blade. The SNS has 4 neurons identified as V1, V2, V3, and V4. Damage was predicted in locations 1 through 5.

4.0 Prototype Sensor System Development

A dedicated local processor is a key component in the SHM system. A local processor architecture was designed to work with the continuous sensor. This processor, different than the SNS, is designed with a local storage of sensor data and a digital bus to download the data. Development of the software emulator for the local processor was done in this project. The emulator work was funded by leveraging a grant to North Carolina A&T State University from the Air Force Materials Laboratory. A semiconductor development company, Triad Semiconductor assisted in the work.

Two different versions of this emulator were successfully tested to monitor fatigue cracks in complex joints in metallic structures. Based on the availability of future funds it is planned to develop the local processor chip based on this architecture. Such a chip can autonomously acquire and analyze AE signals, and to communicate the reduced data over a digital bus. It is possible to embed or surface mount this local processor chip close to the continuous sensor on the structure being monitored. The development of this chip involves several steps before the processor could be miniaturized to a level where it can be integrated into the structure.

5.0 Using a Continuous Sensor to Monitor Fatigue Damage

The continuous sensor performance was analyzed and validated using simulated AE signals, namely those caused by pencil lead breaks. The advantage of the continuous sensor configuration for monitoring actual AE signals generated by fatigue damage growth in a composite specimen was determined. We used 610-mm-long, 25-mm-wide, and 3-mm-thick fiberglass cloth laminate specimens. The central section of the specimen had two semicircular notches of 0.25-inch radii. The specimen was initially subjected to fatigue until a visible crack appeared at one of the edges. The arrangement of sensors on the specimen is shown in Figure 5.1. This specimen was instrumented with a surface-bonded continuous sensor as shown in Figure 5.1. The first node of the continuous sensor was at a distance of 0.625 inches from the fatigue damage site. In addition, two conventional sensors were also attached to the specimen. The sensors S1 and S2 were 0.25-inch damped ultrasonic sensors with a resonant frequency of 5 MHz. These sensors were chosen for their suitability in terms of wide band non-resonant response needed for quantifying AE signals, based on an earlier study.

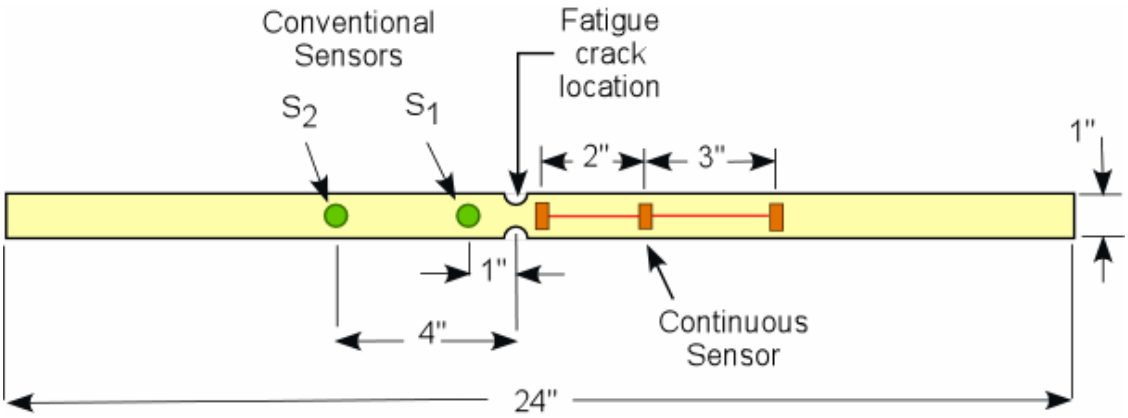

Figure 5.1. Composite specimen with fatigue damage.

The specimen was subjected to a fatigue loading with a mean load of 750 lbs and amplitude of 500 lbs. The test setup is shown in Figure 5.2.

Figure 5.2. Test setup for monitoring the damage growth with a continuous sensor.

Figure 5.3 shows the waveforms of the AE signals obtained during the fatigue loading. The amplitudes of the signals from the continuous sensor were much larger than the signals from the conventional sensor. These differences can be attributed to the frequency responses of the two types of sensors, their relative sizes, and to the fact that surface bonded or embedded sensors are likely to be more sensitive to the AE signals compared to the conventional sensors. The AE signal sensed by the conventional sensors s_2 is much smaller in amplitude compared to that from an identical sensor s_1, which is merely 3 inches closer to the damage site. Furthermore, the high-frequency components present in the signal from s_1 are absent in the signals from the sensor s_2. This variation in the signal characteristics over as short a distance as 3 inches in composite media illustrates the need for multiple sensor nodes in critical regions for the accurate detection of damage magnitudes and rates.

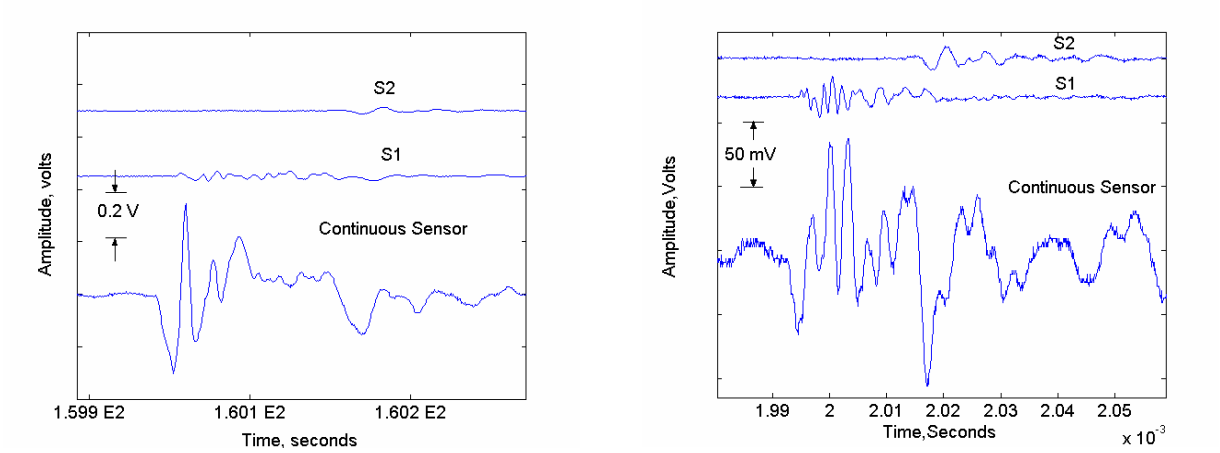

Figure 5.3. Comparison of AE waveforms obtained by a continuous sensor and conventional sensors.

Panels with continuous sensors were developed for verification of the SHM technique. The work included the development of loading fixtures, panels, and the sensor configurations. Glass cloth/polyester composite panels with central circular holes were prepared. A 6-mm slit at the end of one of the horizontal diameters was cut to initiate localized fatigue damage in these panels. These panels were subjected to fatigue loading until a fatigue crack on the order of 0.5 mm was initiated at the end of the notch. These panels were all instrumented with surface mounted continuous sensors.

5.1 Development of Techniques for Damage Assessment and Prognosis

AE-based proof testing on an initial group of about 30 glass cloth/polyester composite coupon specimens was performed. The procedure included the following steps:

1. Determine the cyclic load amplitude under which high-quality specimen lasts at least a million cycles.
2. In a group of specimens that include high-quality specimens as well as defective specimens, apply the proof test procedure developed earlier, and from the results of the proof test it may be possible to separate out defective specimens from the good quality specimens even before the specimens are subjected to extensive fatigue loading.
3. Subject all the specimens to the fatigue cycling determine the actual fatigue durability of each specimen.
4. Find the correlation between the predictions of the AE proof test and the actual fatigue durability.

For the 30 specimens that were tested in the initial tests, it was found that the maximum cyclic load of 60% of static strength was too high and resulted in premature failure of even good-quality specimens. The undamaged coupons failed in the range of about 5,000 to 35,000 cycles. The limited AE data obtained from these specimens did show some trends indicating the usefulness of AE data. However, the experiments had to be repeated at lower cyclic load amplitude with additional specimens and it was found that the load amplitude had to be reduced to 48% of the static strength for the specimens to last an average of one million cycles. These experiments for established the AE-based proof test procedure for prediction of the durability of blade materials.

In an earlier study [15] the AE technique was used with reasonable success for predicting the fatigue durability of carbon fiber thermoplastic hip prostheses. The technique involved tailoring the AE monitoring technique to capture the crucial damage-related events occurring during the fatigue degradation of the composite structural member. Specifically, the AE was recorded during the proof test shown in Figure 5.4. The fatigue life for these specimens varied over 3 decades, and from the AE data obtained prior to the fatigue loading it was possible to differentiate the good composite specimens from those that failed prematurely in the fatigue loading.

This technique is now being reapplied for the prediction of fatigue durability of composite coupon specimens using distributed sensors. Figure 5.5 shows the cumulative AE energy recorded during the initial static loading of the coupon specimens. After the initial static loading to 50% of the nominal static strength, the specimens were cyclically loaded for 10,000 cycles to a maximum stress of 50% of the static strength. At the end of this cyclical load, the specimen was subjected to a proof load reaching a maximum of 60% of static load. AE signals during this stage were recorded. Finally, the specimens were loaded in fatigue at 60% of nominal static strength until failure.

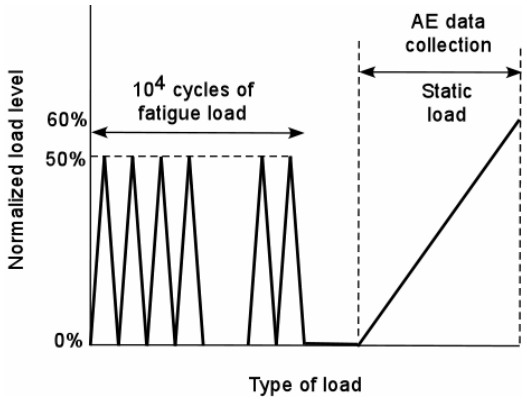

Figure 5.4. AE proof test procedure [15].

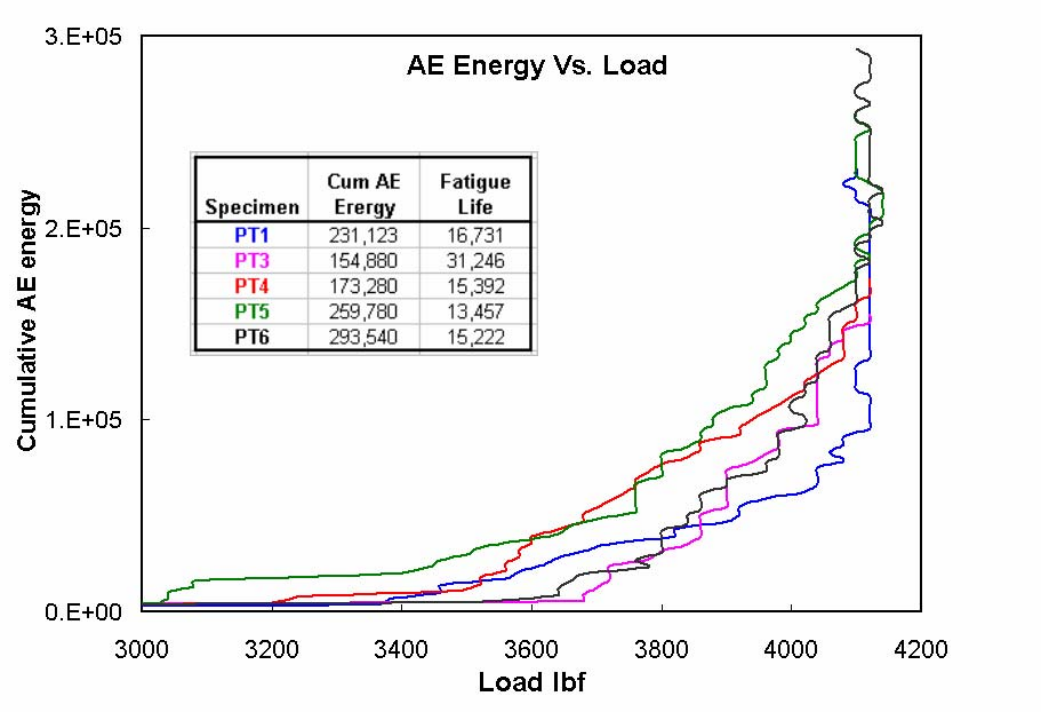

Figure 5.5. AE energy from composite coupons during initial static loading.

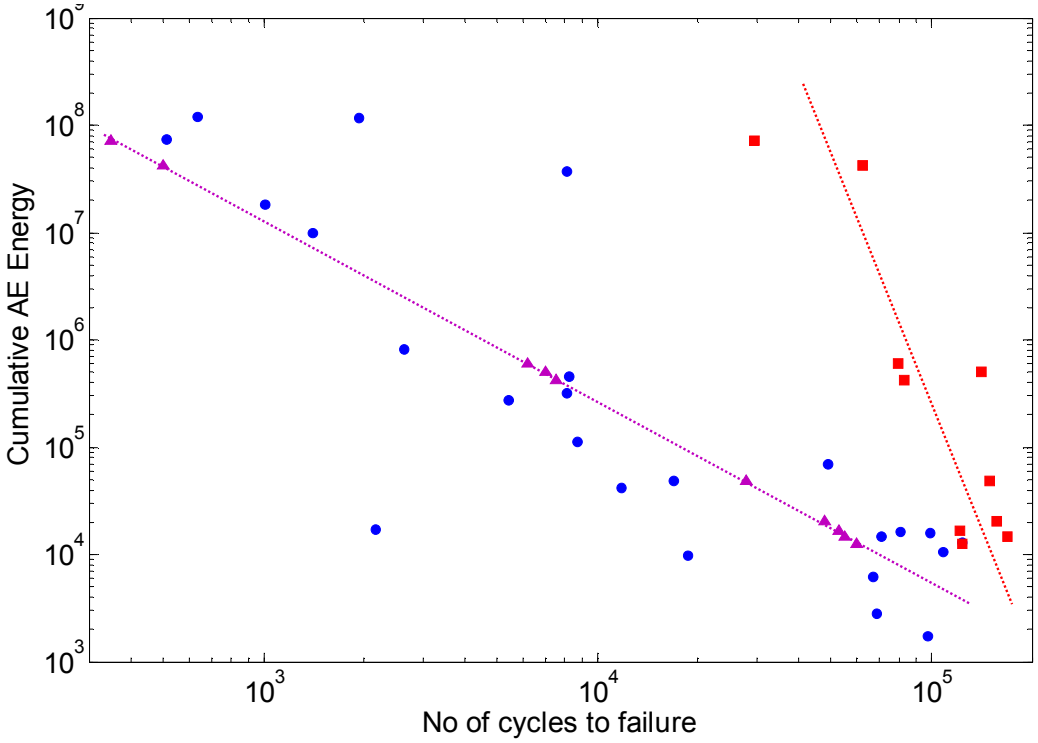

Figure 5.6. Estimation of fatigue durability of woven glass fiber epoxy composite coupon specimens; blue circles represent specimens used for establishing the trend of AE energy vs. life; the five pink triangles represent the specimens whose fatigue life was estimated at 50% of static strength; red squares represent the actual fatigue life of these five specimens at reduced fatigue load (40% of static strength instead of 50% of static strength).

The relationship between the AE parameters and fatigue durability was established. Based on the life estimations from this data, fatigue load amplitudes could be suitably modified to extend the coupon lives to desired lengths. During the reported period, additional coupons were tested to validate the trend in the life extensions.

The relationship between the AE energy generated during a proof testing procedure that precedes the fatigue testing and the fatigue life subsequently measured for nominally similar specimens has been established. Some of these specimens were machined specimens while others had two different levels of impact damage. Specimens in each category had orders of magnitude variability in fatigue life and the three categories overlapped in terms of their fatigue durability. This test program involved developing the proof testing procedure, testing nearly 50 specimens both through the proof tests and fatigue durability tests. As shown in figure 5.6, reasonably good correlation between the total AE energy during the proof tests and the fatigue life is seen, considering that both the life and AE energy span over 3 orders of magnitude. The specimens used to generate the correlation between the AE energy and the fatigue life are shown as blue circles. The next step is to make use of this new information that can be used to estimate the fatigue durability of nominally similar specimens. There are two ways in which this information could be potentially useful.

- One of the important difficulties in designing structural members for fatigue life is that the design is driven by the weakest members of the population and hence is over conservative. Any information on the estimated life of *individual members* can reduce the conservatism and thus make the systems lighter and less expensive.

- We can improve the survivability of a part after it has been damaged. If an individual turbine blade is estimated to have shorter fatigue life under the design loads, it may be possible to reduce the operating load by a small fraction (often only 5 to 10% reduction is required) to make it survive the designed life. This approach to life extension is currently being studied. Five more specimens were subjected to impact damages and taken through the proof testing procedure to estimate their fatigue life. With the intention of extending the life of weaker specimens, they were subjected to reduced fatigue loads. These specimens were subjected to 40% of static strength instead of the 50% of static strength that was used to generate the AE Energy versus Life trend until they failed.

This testing has shown that in a laboratory setting it is possible to estimate the life of coupons subjected to varying degrees of damage, and use this information to extend their life through appropriate reduction in their operating load so that the coupons survive for design life.

6.0 Monitoring the Onset of Buckling

Experiments were carried out to detect incipient buckling in simple laboratory experiments. These experiments were the continuation of earlier wind turbine blade tests at the National Wind Energy Center, when the potential of using the stress wave propagation technique for detecting incipient buckling was identified. These experiments are described below.

6.1. Composite Bar Subjected to Buckling

The experiments described in this section used vibration/stress wave monitoring for the detection of buckling under more controlled conditions. A composite bar 2 inches wide and 0.125 inch thick was instrumented with two PZT patches as shown in Figure 6.1. This specimen was first supported in the straight unbuckled condition as shown. The ends were clamped using 0.25 x 2.5 x 6-inch plates. The left end of the bar was kept stationary while the right end of the plate was translated to introduce the desired level of buckling. The central buckling displacement was measured using a ruler. Rubber sheets were introduced between the metal plates at the clamped ends so as to nearly eliminate the waves from being reflected at the ends. The clamping force was accurately controlled using torque wrenches. The clamping steel plates at each end were held by five individual steel bolts and each of these bolts was tightened to the same level of torque (15 ft-lbs) as the bar was taken through different levels of buckling. The instrumentation used for introducing vibration into the specimen and for monitoring the amplitude of the vibrations is shown in Figure 6.2. It consisted of an arbitrary function generator and a power amplifier, which delivered gated sine pulses to the transmitting PZT patch on the bar. The signal from the receiving PZT patch was collected directly in a digital oscilloscope and transferred to the personal computer (PC). In the first set of experiments, various exciting frequencies ranging from 40 Hz to 15 kHz were examined. One of the frequencies that provided good indications of the buckling deformation was 72 Hz. The exciting pulse was a Guasian sine pulse consisting of two complete cycles of sine waves at 71 Hz created in an arbitrary function generator with an amplitude of 9 volts. This pulse was amplified by a power amplifier by a factor of 20 before being applied to the PZT patch on the left side of the specimen.

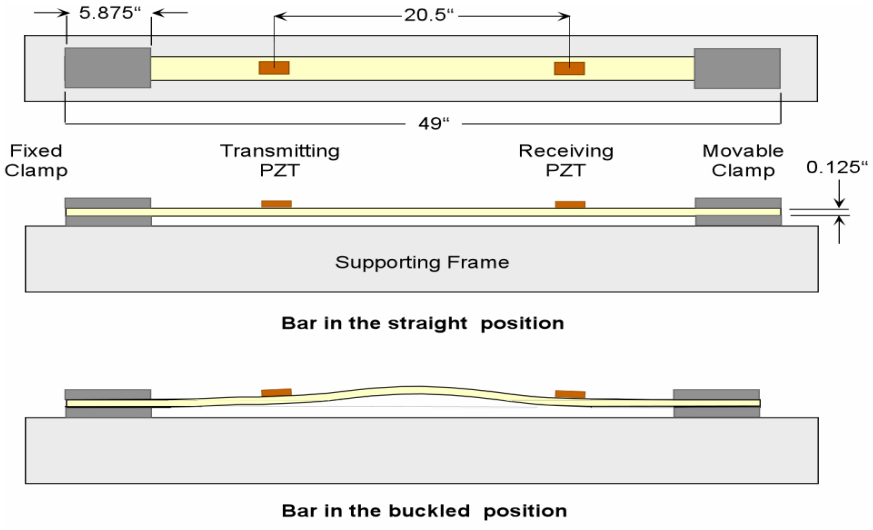

Figure 6.1. Specimen used for buckling experiments.

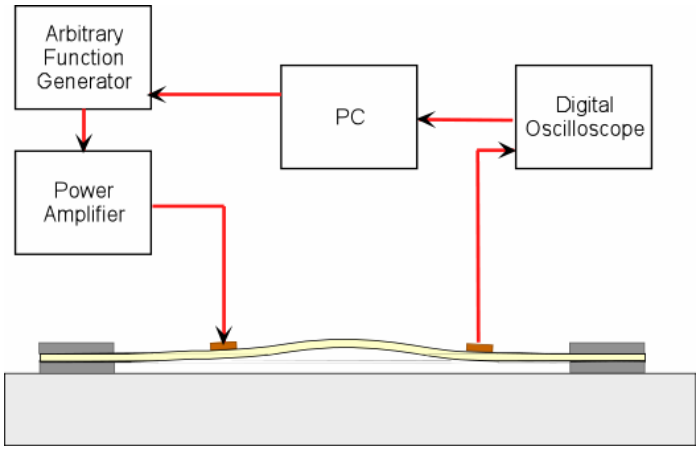

Figure 6.2. Instrumentation used for measuring the specimen response.

The signals from the receiving PZT patch were recorded when the buckling induced deflection at the mid point of the bar was 0.2 inch (0.5 cm), 0.4 inch (1.0 cm), 0.69 inch (1.75 cm), and 1.0 inch (2.5 cm). Finally, the bar was returned to its original unbuckled state and the vibration amplitude was again measured. Figure 6.3 shows the comparison of the waveforms corresponding to the unbuckled state and various buckled states. The magnitude of the oscillations undergoes a drastic reduction as the buckling displacement increases. These changes are apparent even at the early stages of buckling when the central displacement is of the order of 0.25 inch. When the bar was returned to the unbuckled state, the signal amplitude returned to the initial unbuckled bar amplitude as seen from Figure 6.3, indicating that the changes in amplitude are indeed caused by the buckling deformation in the bar. In a second experiment, the bar was excited by sinusoidal chirp signals with various starting and ending frequencies. The results corresponding to a 3-second chirp with a starting frequency of 60 Hz and ending frequency of 120 Hz is shown in Figure 6.4.

It is possible to estimate the resonant frequencies of the bar in the different stages of buckling from the horizontal positions of the peaks in the response curves. The frequency of oscillation at time t = 0, 1, 2, and 3 seconds are respectively 60, 80, 100, and 120 Hz. In general it could be seen that as the buckling deformation increases, the frequency of maximum amplitude for the bar, which originally was at about 76 Hz, gradually increased until it reached 112 Hz. However, when the displacement of mid point of the bar increased from 0.0 to 0.2 inch (0.5 cm), the resonant frequency appeared to fall to about 68 Hz. As the buckling displacement increased from this value on, the general trend described above was followed.

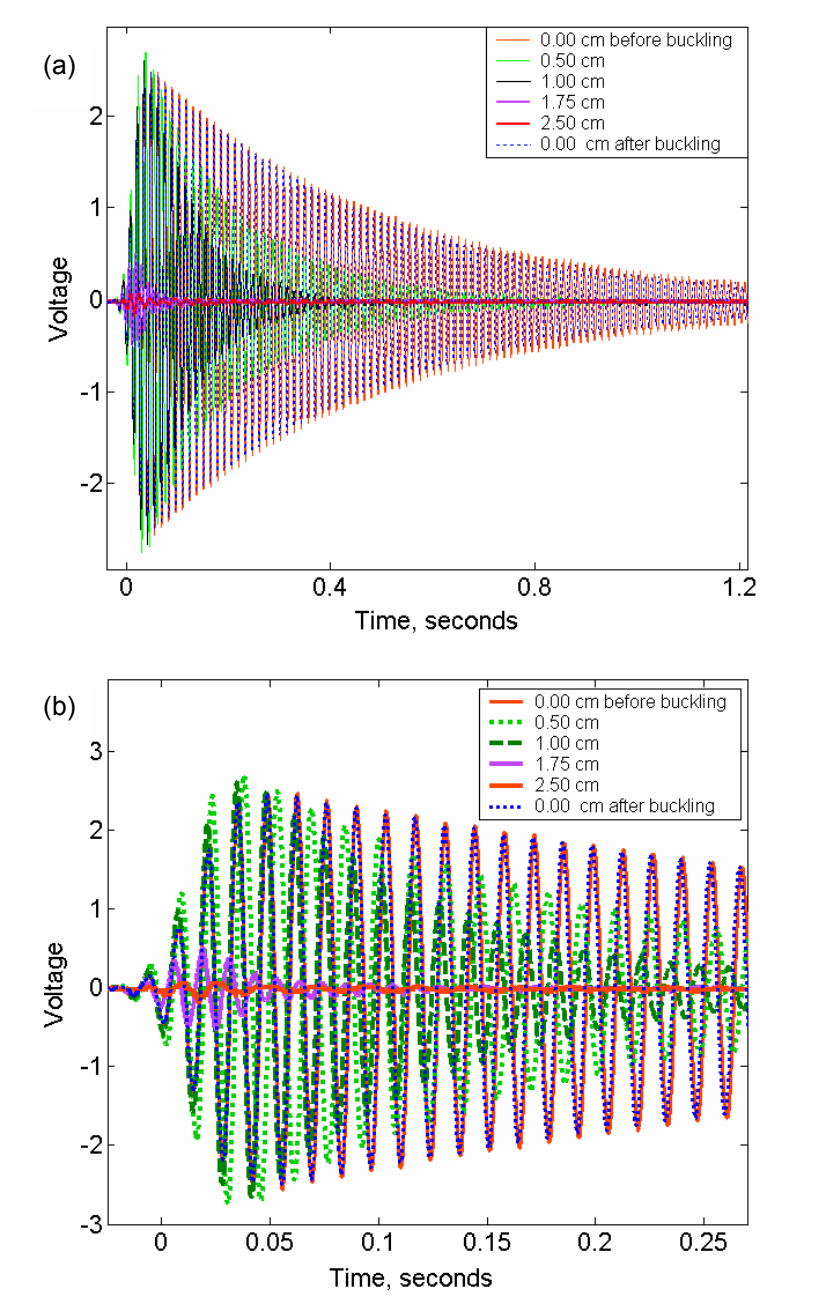

Figure 6.3. Comparison of waveforms obtained in the unbuckled and buckled condition; (a) the complete waveforms, and (b) the initial portion of the waveforms expanded.

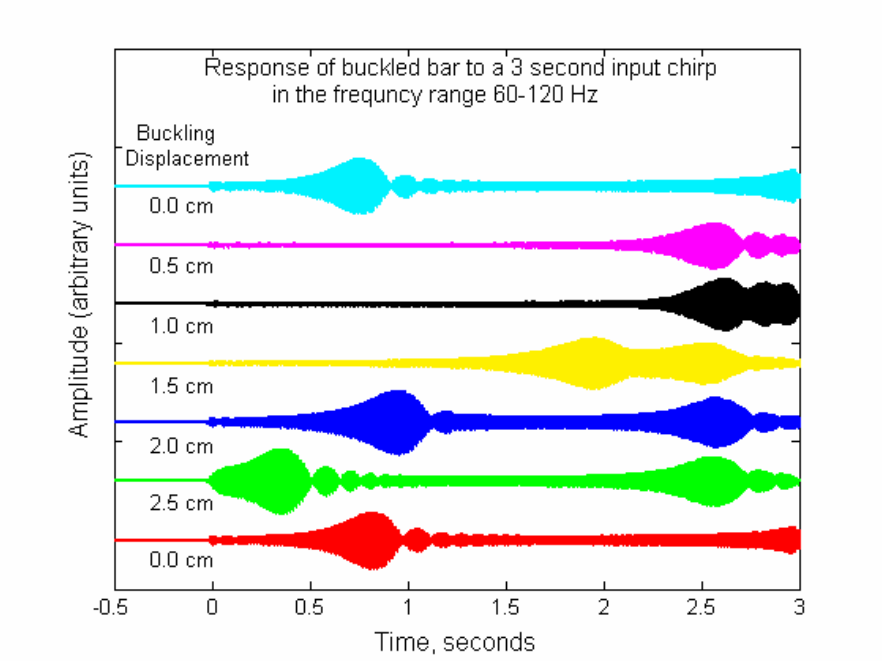

Figure 6.4. Response of the buckled bar to chirp excitation.

6.2 Summary

In this section a vibration-based technique for detecting the onset of buckling in bars is described. Since buckling can lead to damage to the materials as well as catastrophic failure of the structure, the technique described is likely to be of interest in health monitoring applications. The simple experiment described indicates that it is possible to remotely detect even early stages of buckling-related deformation. Further study of the interaction between the vibration characteristics and buckling deformation is necessary to formalize this technique and is being pursued.

7.0 Design of the Smart Blade

The smart blade could be coupled to a remote monitoring station that would log health information from the wind turbine. An approach has also been outlined to make the intelligent blade autonomous. The PZT nerves are already self-powered, and the AFC material can also be used for micro power generation to power the TBIM for signal processing. Wireless transmission of the reduced health information could simplify the health monitoring system. It is estimated that signal processing electronics on each blade might require on the order of 10 watts of power to operate. This could be achieved by harvesting strain energy in the blades produced by the gravity moments and the wind loading. The improved reliability, reduced maintenance, and increased wind capture would make the smart blade cost effective. The concept for the smart blade is shown in Figure 7.1.

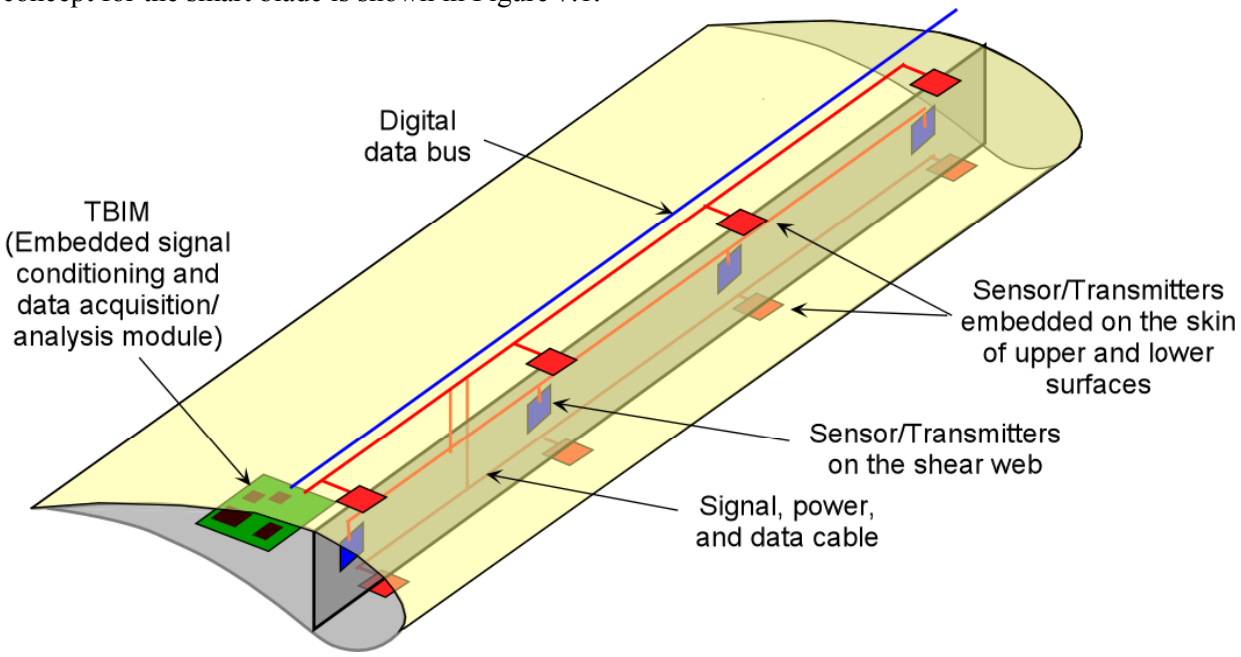

Figure 7.1. Initial design for a smart blade.

8.0 Conclusions

Modeling, simulation, and experimentation have shown the feasibility of detecting damage in composite structures using continuous sensors in different arrangements. The algorithms developed in this work are based on detecting damage using a minimum number of channels of data acquisition. In developing the algorithms, we considered the cost, the large size of the blades, and the fact that the system must operate for 30 years. The test results obtained in this project indicate that health monitoring using continuous sensors is a practical technique for monitoring the condition of large structures. Vibration, AEs, and strains can be measured using the distributed sensors. The development of a smart blade that uses continuous sensors and microelectronics to mimic the biological nervous system is the eventual goal of the research. Testing of continuous sensors showed that they were capable of detecting AEs on large composite structures and simultaneously reducing the number of channels of data acquisition. The sensor system for the smart blade was developed in this project. It is hoped that a prototype smart blade can be built and tested with collaboration of NREL, a blade manufacturer, and Sandia National Laboratory.

9.0 References

1. Kirikera, G., *An Artificial Neural System for Structural Health Monitoring.* MS Thesis, Cincinnati, OH: University of Cincinnati, August 2003.
2. Datta, S., *An Active Fiber Continuous Sensor for Structural Health Monitoring.* MS Thesis, Cincinnati, OH: University of Cincinnati, August 2003.
3. Sundaresan, M.J.; Schulz, M.J.; Ghoshal, A.; Pratap, P. "A Neural System for Structural Health Monitoring," SPIE 8th International Symposium on Smart Materials and Structures, San Diego, CA, March 4−8, 2001.
4. Bent, AA; Hagood, N.W "Piezoelectric fiber composite with Interdigitated Electrodes," *J. Intell. Mater. Syst. Struct*., Vol. 8, 1998.
5. CeraNova Corporation, 101 Constitution Boulevard, Suite D, Franklin, MA 02038-2587. Online www.ceranova.com/products.htm, 2006.
6. Wilkie, W.K.; Bryant, R.G.; High, J.W.; Fox, R.L. Hellbaum, R.F. Jalink, A.; Little, B.D.; Mirick, P.H. "Low Cost Piezocomposite Actuator for Structural Control Applications." SPIE 7th Annual International Symposium on Smart Structures and Materials, Newport Beach, CA, March 5−9, 2000.
7. Martin, W.N.; Ghoshal, A.; Schultz, M.J.; Sundaresan, M. J. "Structural Health Monitoring Using an Artificial Neural System," *Recent Research Developments in Sound and Vibrations. Transworld Research Network*, 2002.
8. Schulz, M.J.; Chattopadhyay, S.; Sundaresan, M.J; Ghoshal, A.; Martin, W.N.; Pratap, P.R.; "Processing, Understanding and Applications of Piezoceramic Materials for an Artificial Neural System." Ceramic Materials Symposium at the International Mechanical Engineering Congress and Exposition, Winter Annual Meeting of the ASME, New York, NY, Nov. 11−16, 2001.
9. Cady, W.G. *Piezoelectricity: an introduction to the theory and applications of electromechanical phenomenon in crystals*. Dover, NY, 1964.
10. Kirikera, G;Shultz, M.J.; Ghoshal, A.; Sundaresan, M.J.; Feaster, J.; Hughes, D. "Recent Advances in an Artificial Neural System for Structural Health Monitoring," SPIE 10th International Symposium on Smart Materials and Structures, San Diego, CA, March 2−6, 2003.
11. Datta, S.; Kirikera, G.R.; Pammi, S.; Brown, C.; Schulz, M.J.; Sundaresan, M.J. "Continuous Sensors for Structural Health Monitoring," SPIE 10th International Symposium, NDE for Health Monitoring and Diagnostics, San Diego, CA, March 2−6, 2003.
12. Muralt, P., *Piezoelectric Thin Films for MEMS*, Laboratoire de Ceramique, Federal Institute of Technology, Lausanne, Switzerland, 1997.
13. Wan, J.G.; Tao, B.Q. "Design and Study on a 1-3 Anisotropic Piezocomposite Sensor," Nanjing University, Nanjing, PR China, Materials and Design 21, 2001.
14. Ko, W. H. "The Future of Sensor and Actuator Systems," Case Western Reserve University, Cleveland, OH, Sensors and Actuators A56.
15. Sundaresan, M. J.; Henneke, II, E.G.; Reifsnider, K.L. 1994, "Prediction of Fatigue Life of Composite Femoral Prostheses Using Acoustic Emission Technique," *Journal of Composites - Technology and Research*, pp. 127−137.

16. Kirikera, G.; Datta, S.; Westheider, B.; Schulz, M.J.; Sundaresan, M.J.; Martin, Jr., W.N.; Ghoshal, A., "An Artificial Neural System," Invention Disclosure, University of Cincinnati, UC 103-046. August 26, 2003.

17. Datta, S.; Hause, J.; Kirikeria, G.; Hurd, D.; Schulz, M.J.; Sundaresan, M., "An Active Fiber Continuous Sensor," Invention Disclosure, University of Cincinnati, UC 103-034. July 21, 2003.

18. Kang, I.; Lee, J.W.; Yeo-Heung, Y.; Shanov, V.; Schulz, M.J.; "A Multifunctional Carbon Nanotube Neuron for Structural Health Monitoring," Invention Disclosure, University of Cincinnati, UC 105-046. Prepared July 2005. Submitted July 29, 2005.

19. Kirikera, G.; *A Structural Neural System for Health Monitoring of Complex Structures*, Ph.D. Dissertation, University of Cincinnati, Cincinnati, Ohio, 2006.

20. Kirikera, G.R.; Shinde, V.; Schulz, M.J.; Ghoshal, A.; Sundaresan, M.J.; Allemang, R.J.; Lee, J.W. "A Structural Neural System for Real-Time Health Monitoring of Composite Materials,", Submitted for publication February 2006 to Structural Health Monitoring: An International Journal.

21. Kirikera, G.R.; Shinde, V.; Schulz, M.J., Allemang, R.; Sundaresan, M.J.; Ghoshal, A. "A Structural Neural System for Health Monitoring of Composite and Metallic Structures under Ambient Conditions," *Mechanical Systems and Signal Processing*.

22. Shinde, V. *Development of Active Fiber Sensors and a Data Acquisition Module for a Structural Neural System.* MS Thesis. Cincinnati, OH: University of Cincinnati, 2006.

23. Kirikera, G.R.; Schulz, M.J.; Sundaresan, M.J.; Hughes, S.; Gevorgian, V.; VanDam, J.; Nkrumah, F.; Grandhi, G. "Structural Health Monitoring Proof Testing of a Wind Turbine Blade at the National Renewable Energy Laboratory." To be submitted for publication.

10.0 Publications

The following papers have been submitted or published thus far with partial support by the project.

(a) Papers Submitted:

1. Lee, J.W.; Kirikera, G.R.; Kang, I.; Schulz, M.J.; Shanov, V.N. "Structural Health Monitoring using Continuous Sensors and Neural Network Analysis." Submitted June 9, 2005 to *Smart Materials and Structures*. In review.
2. Inpil Kang, Mark J. Schulz, Jay H. Kim, Vesselin Shanov, Donglu Shi, *A Carbon Nanotube Strain Sensor for Structural Health Monitoring*, Volume 15, Number 3, June 2006, Smart Materials and Structures.
3. Kirikera, G.R.; Shinde, V.; Schulz, M.J.; Allemang, R.; Sundaresan, M.J.; Ghoshal, A.; "A Structural Neural System for Health Monitoring of Composite and Metallic Structures under Ambient Conditions." Accepted, *Mechanical Systems and Signal Processing*.
4. Kang, I.; Heung, Y.Y.; Kim, J.H.; Lee, J.W.; Gollapudi, R.; Subramaniam, S.; Narasimhadevara, S.; Hurd, D.; Kirikera, G.R.; Shanov, V.; Schulz, M.J.; Shi, D.; Boerio, J.F.; Mall, S.; Ruggles-Wren, M.; "Introduction to Carbon Nanotube and Nanofiber Smart Materials," *Composites B Journal, 37* 2006.
5. Elwasia, N.; Sundaresan, M.J.; Schulz, M.J.; Ghoshal, A.; Pai, P.F.; Tu, P.K.C. "Damage Bounding Structural Health Monitoring," *Journal of Intelligent Materials and Smart Structures*, in press.

(b) Papers published in peer-reviewed journals:

1. Martin Jr., W. N.; Ghoshal, A.; Sundaresan, M. J.; Lebby, G.; Pratap, P.R.; Schulz, M. J. "An Artificial Neural Receptor System for Structural Health Monitoring," *Structural Health Monitoring: An International Journal*; Vol. 3, No 3, 2005.
2. Hughes D. R.; Ghoshal A.; Rowe, E.; Sundaresan, M.J.; Schulz, M.J.; Feaster, J.T. "Health Monitoring of Thick Materials Using Piezoceramic Patches, Time signals and Wavelet Transmittance Functions," *J. of Shock and Vibration*; Vol. 11, No. 1, 2004, pp. 47−66.
3. Schulz, M.J.; Sundaresan, M.; McMichael, J.; Clayton, D.; Sadler, R.; Nagel, W.; "Piezoelectric Materials at Elevated Temperature," *J. Intelligent Material Systems and Structures;* Vol. 14, No 11, November 2003, pp. 693−705.
4. Schulz, M.J.; Ghoshal, A.; Sundaresan, M.J.; Pai, P.F.; Chung, J.H. "Theory of Damage Detection using Constrained Vibration Deflection Shapes," *Structural Health Monitoring: An International Journal;* Vol. 2, No. 1, March 2003.
5. Sundaresan, M.J.; Ghoshal, A.; Lia, J.; Schulz, M.J.; Pai, P.F.; Chung, J.H.; "Experimental Damage Detection on a Wing Panel Using Vibration Deflection Shapes," *Structural Health Monitoring: An International Journal,* Vol. 2, No. 3, 2003.

(c) Papers published in non-peer reviewed journals or conference proceedings:

1. Kirikera, G.; Shinde, V.; Kang, I.;Schulz, M.J.; Lee, J.W.; Ghoshal, A.; Sundaresan, M.J. "A Dual Mode Active/Passive Structural Neural System." International Workshop on Structural Health Monitoring, Stanford, CA: Stanford University, September 12−14, 2005.
2. Kirikera, G.R.; Kang, I.P.; Lee, J.W.; Shinde, V.; Westheider, B.; Shanov, V.; Schulz, M.J.; Sundaresan, M.; Ghoshal, A. "Testing the Analog Processor of a Structural Neural System." SPIE Smart Structures Conference, San Diego, CA, March 6−10, 2005.
3. Shinde, V.; Kirikera, G.; Schulz, M.; Datta, S.; Westheider, B.; Hurd, D.; Hause, J.; Gilliland, R.; Sundaresan, M.J. "An Experimental Structural Neural System," Eleventh International Conference on Composites/Nano Engineering, ICCE-11 August 8−14, 2004 in Hilton-Head Island, South Carolina, USA.
4. Sundaresan, M.; Kemerling, J.; Nkrumah, F.; Grandhi, G.; Schulz, M.J. "Evaluation Of A Scalable Structural Health Monitoring System Based on Acoustic Emission Sensing," *European Workshop on SHM*, Munich Germany, July 7−9, 2004.
5. Sundaresan; Nkrumah, F.; Grandhi, G.; Schulz, M. "Identification of Failure Modes Using Continuous AE Sensor System," Proceedings of the 2004 International Mechanical Engineering Congress and Exposition, Anaheim, CA, American Society of Mechanical Engineers, New York, NY.
6. Ali, B.; Sundaresan, M.; and Schulz, M. "Early Detection of Local Buckling in Structural Members," ASME International Mechanical Engineering Congress, Anaheim, CA, November 13−19, 2004.
7. Sundaresan, M.; Grandhi, G.; Schulz, M.J.; Kemerling, J.C. "Monitoring Damage Growth in a Composite Plate Using a Continuous Sensor." January 26−29, 2004, Dearborn, MI, USA.
8. Kirikera, G.R.; Datta, S.; Schulz, M.J.; Ghoshal, A.; Sundaresan, M.J. "Mimicking the Biological Neural System Using Active Fiber Continuous Sensors and Electronic Logic Circuits," SPIE 11th International Symposium on Smart Structures, San Diego, CA, March 2004.
9. Sundaresan, M.J.; Grandhi, G.; Uitenham, L.; Schulz, M.J.; Kemerling, J.; Hughes, J.; "Development of an Acoustic Emission Based Structural Health Monitoring System," Fourth International Workshop on Structural Health Monitoring, September 15−17, 2003, Stanford, CA: Stanford University.
10. Sundaresan, M.J.; Grandhi, G.; Schulz, M.J. "A Structural Health Monitoring System Based On Continuous Acoustic Emission Sensors," Quantitive Nondestructive Evaluation Conference, Green Bay, Wisconsin, July 27−August 1, 2003.
11. Kirikera, G.; Datta, S.; Hause, J.; Westheider, B.; Schulz, M.J.; Ghoshal, A.; Sundaresan, M.J.; Pratap, P. "Mimicking the Biological Neural System," ICCE-10 Conference, New Orleans, LA, July 20−26, 2003.
12. Datta, S.; Hause, J.; Kirikera, G.; Hurd, D.; Schulz, M.J.; Sundaresan, M.J.; Ghoshal, M.J. "A Continuous Sensor for Ultrasensitive Acoustic Monitoring," ICCE-10 Conference, New Orleans, LA, July 20−26, 2003.
13. Pammi, S.L.; Brown, C.; Kang, I.; Jain, S.; Hurd, D.; Narasimhadevara, S.; Mokashi, V.; Liu, Y.; Schulz, M.J.; Chase, J.; Kaul, P.;He, P.; Yang, L.; Xiao, F.; Shi, D.; Boerio, J.; "Multifunctional Materials using Carbon Nanotubes," ICCE-10 Conference, New Orleans, LA, July 20−26, 2003.

14. Grandhi, G.; Sundaresan, M.; Schulz, M.; "Monitoring of Damage Evolution in Composite Laminates with Distributed Sensors," ICCE-10 Conference, New Orleans, LA, July 20−26, 2003.

15. Ali, B.; Sundaresan, M.; Gurunathan, S.; Ferguson, F.; Schulz, M. "Early Detection of Structural Instability," ICCE-10 Conference, New Orleans, LA, July 20−26, 2003.

16. Elwasila, N.; Sundaresan, M.; Schulz, M.; Sankar, J. "A Damage Vector Method for Structural Health Monitoring of Bars and Beams," ICCE-10 Conference, New Orleans, LA, July 20−26, 2003.

17. Datta, S.; Kirikera, G.; Schulz, M.J.; Ghoshal, A.; Sundaresan, M.J. "An Active Fiber Continuous Sensor," Fourth International Workshop on Structural Health Monitoring, September 15−17, 2003, Stanford, CA: Stanford University.

18. Kirikera, G.; Datta, S.; Schulz, M.J.; Ghoshal, A.; Sundaresan, M.J. "An Artificial Central Nervous System for Structural Health Monitoring of Orthotropic Materials," Fourth International Workshop on Structural Health Monitoring, September 15−17, 2003, Stanford, CA: Stanford University.

19. Ghoshal, A.; Prosser, W.H.; Kirikera, G.; Schulz, M.J.; Hughes, D.; Orisamolu, W. "Concepts and Development of Bio-Inspired Distributed Embedded Wired/Wireless Sensor Array Architectures for Acoustic Wave Sensing in Integrated Aerospace Vehicles," Fourth International Workshop on Structural Health Monitoring, September 15−17, 2003, Stanford, CA: Stanford University.

20. Sundaresan, M.; Ali, B.; Uitenham, L.; Ferguson, F.; Schulz, M.J.; "Development of Health Monitoring Techniques for the Detection of Incipient Buckling In Aerospace Structures," Fourth International Workshop on Structural Health Monitoring, September 15−17, 2003, Stanford, CA: Stanford University.

21. Sundaresan, M.; Uitenham, L.; Grandhi, G.; Uppaluri, S.; Schulz, M.J. "Evaluation of Failure Modes and Fatigue Durability of Structural Members Using Embedded Instrumentation." Fourth International Workshop on Structural Health Monitoring, September 15−17, 2003, Stanford, CA: Stanford University.

22. Datta, S.; Kirikera, G.; Sundaresan, M.J.; Schulz, M.J. "Active Fiber Composite Continuous Sensors," International Conference on Smart Materials, Structures and System (ISSS-SPIE 2002), December 12−14, 2002, Bangalore, India.

23. Sundaresan, M.; Grandhi, G.; Schulz, M.; Kirikera, G. "Embedded Continuous Sensor for Monitoring Damage Evolution in Composite Materials," SPIE Conference on Smart Structures, Devices, and Systems, RMIT University, December 16−18, 2002, Melbourne, Australia.

24. Sundaresan, M.; Ali, B.; Ferguson, F.; Schulz, M.J."Early Detection of Local Buckling In Composite Bars," SPIE Conference on Smart Structures, Devices, and Systems, RMIT University, December 16−18, 2002, Melbourne, Australia.

25. Pammi, S.; Brown, C.; Datta, S; Kirikera, G.R.; Schulz, M.J.; Kaul, P.; He, P.; Shi, D.; Boerio, F.J.; . Sundaresan, M.J. "Building Artificial Nerves for Structures," IMECE2002-33475, Proceedings of IMECE'02 2002 ASME International Mechanical Engineering Congress & Exposition, New Orleans, LA, November 17−22, 2002.

26. Schulz, M.J.; Sundaresan, M.J.; McMichael, J.; Clayton, D. "Evaluation of the Performance of Piezoceramic Materials at Moderately Elevated Temperatures," IMECE2002-34376, Proceedings of IMECE'02 2002 ASME International Mechanical Engineering Congress & Exposition, New Orleans, LA, November 17−22, 2002.

27. Sundaresan, M.J.; Schulz, M.J.; "Sensory Systems for Assessing Damage Growth in Composite Materials," Ninth International Conference on Composites Engineering, July 1−6, 2002, San Diego, CA.
28. Elwasila, N.; Sundaresan, M.J.; Sankar, J.; Schulz, M.J.; "A Vibration Based Technique for Detecting Damage in Composite Bars," Ninth International Conference on Composites Engineering, July 1−6, 2002, San Diego, CA.
29. Gangadhararao, G.; Sankar, J.; Sundaresan, M.J.; Schulz, M.J. "Assessing Damage Growth in Composite Materials Using a Continuous Sensor," Ninth International Conference on Composites Engineering, July 1−6, 2002, San Diego, CA.
30. Ali, B.; Ferguson, F.; Sundaresan, M.J.; Schulz, M.J. "Monitoring the Onset of Column Instability Using Stress Wave Propagation," Ninth International Conference on Composites Engineering, July 1−6, 2002, San Diego, CA.
31. Ferguson, F.; Sundaresan, M.J.; Grandhi, G.; Datta, S.; Kirikera, G.R.; Schulz, M.J. "Evaluation of a Neural System for Structural Health Monitoring," First European Workshop on Structural Health Monitoring, Ecole Normale Supérieure, Cachan, Paris, July 10−12, 2002.
32. Ghoshal, A.; Martin, W.N.; Schulz, M.J. "Simulation of Asymmetric Lamb Wave Propagation for Health Monitoring," First European Workshop on Structural Health Monitoring, Ecole Normale Supérieure, Cachan, Paris, July 10−12, 2002.
33. Datta, S.; Kirikera, G.R.; Schulz, M.J.; Sundaresan, M.J. "Sensor Design for an Artificial Neural System," Ninth International Conference on Composites Engineering, July 1−6, 2002, San Diego, CA.
34. Kirikera, G.R.; Datta, S.; Schulz, M.J.; Sundaresan, M.J. "An Artificial Neural System for Health Monitoring of Large Structures," Ninth International Conference on Composites Engineering, July 1−6, 2002, San Diego, CA.
35. Schulz, M.J.; Kirikera, G.R.; Datta, S.; Sundaresan, M.J. "Piezoceramic and Nanotube Materials for Health Monitoring," SPIE Conference, San Diego, CA, March 18, 2002.
36. Ghoshal, A.; Martin, W.N.; Schulz M.J.; Chattopadhyay, A.; Prosser, W.H. "Wave Propagation Sensing for Damage Detection in Plates," SPIE Conference, San Diego, CA, March 18, 2002.
37. Martin, W.N.; Ghoshal, A.; Sundaresan, M.J.; Schulz, M.J.; Lebby, G. "Artificial Neural System for Structural Monitoring," SPIE Conference, San Diego, CA, March 18, 2002.

Book Chapter:

1. Martin, W.N.; Ghoshal, A.; Sundaresan, M.J.; Schulz, M.J.; "Structural Health Monitoring Using an Artificial Neural System," *Recent Research Developments in Sound and Vibration*, Transworld Research Network, Reference number TRN/SV/UA/S0008, 2003.

SME Technical Paper:

1. Datta, S.; Kirikera, G.R.; Schulz, M.J.; Sundaresan, M.J. "Sensor Design for an Artificial Neural System," published by the Society of Manufacturing Engineers (SME), Dearborn, MI, as an SME Technical Paper, EE02-314, December 2002. This paper is disseminated in hard-copy form, on microfiche, and electronically through SME's Web site.

11.0 Undergraduate Student Design Project

Students in one section of the undergraduate Machine Analysis and Design course MECH 321, taught at the University of Cincinnati, participated in a wind turbine design project for the period 2002 to 2004. Mark Schulz teaches this course to all the UC Mechanical Engineering Students at the University of Cincinnati. Each year about 30 of the 75 pre-junior students form project groups of three students per group and each group designs the low speed shaft of a horizontal axis wind turbine. Mr. Alan Laxson of NREL was the technical monitor of this project and helped us obtain information for the design of the wind turbines by allowing us to get design information from Mr. David Malcolm. Mr. Malcolm provided much information and advice on wind turbine design. The shaft design is based on loading for a 1.5MW turbine. The design analysis used the Distortion Energy-Gerber method for predicting fatigue life under combined loading with fluctuating and mid-range stresses. The students came up with some unusual preliminary designs for wind turbine shafts. These included hollow shafts to minimize weight, hollow tapered shafts to minimize weight by maintaining a uniform stress level along the shaft, and shafts made of different metals and composite materials. The students also suggested that the blade and hub might be redesigned to move the blade closer to the bearing to reduce the bending stress due to the weight of the blades and hub.

Contact information for Mr. Laxson and Mr. Malcolm follows.

Alan Laxson
National Renewable Energy Laboratory
1617 Cole Blvd.
Golden, CO 80401
E-mail: alan_laxson@nrel.gov

David Malcolm
Global Energy Concepts, LLC
5729 Lakeview Drive NE, Suite 100
Kirkland, Washington 98033-7340
Phone: 425-822-9008 Ext 17
Fax 425-822-9022
E-mail: dmalcolm@globalenergyconcepts.com

12.0 Acknowledgments

The grant technical monitor for this project is Mr. Alan Laxson. His efforts in directing the research and providing contacts with other researchers at NREL, Sandia Labs, and in industry are a large factor in the success of the research. The undergraduate students also thank Mr. David Malcolm and Mr. Alan Laxson for providing information on wind turbines for the course design projects. Mr. Scott Hughes, V. Gevorgian, and J. VanDam of NREL participated in the wind turbine testing and made the testing successful.

12.1 Faculty and Staff Working on the Project

The faculty and staff that worked on the project are listed below.

- Mannur Sundaresan, Associate Professor, North Carolina A&T State University
- Douglas Hurd, Machinist, University of Cincinnati
- Mark J. Schulz, Associate Professor; University of Cincinnati.

12.2 Students Supported

The students that were partially supported to work on the project are listed below. The students received support from other projects also.

- Saurabh Datta, Goutham Kirikera, SriLaxmi Pammi, Inpil Kang, graduate students, University of Cincinnati
- Jacob Hause (co-op student with outside leveraged support), undergraduate student, University of Cincinnati
- Gangadhararao Grandhi, Bashir Ali, North Carolina A&T State University.

REPORT DOCUMENTATION PAGE

Form Approved
OMB No. 0704-0188

PLEASE DO NOT RETURN YOUR FORM TO THE ABOVE ORGANIZATION.

1. REPORT DATE *(DD-MM-YYYY)*	2. REPORT TYPE	3. DATES COVERED *(From - To)*
August 2006	Subcontract report	May 30, 2002 - April 30, 2006

4. TITLE AND SUBTITLE
A Smart Sensor System for Structural Condition Monitoring of Wind Turbines

5a. CONTRACT NUMBER
DE-AC36-99-GO10337

5b. GRANT NUMBER

5c. PROGRAM ELEMENT NUMBER

6. AUTHOR(S)
M.J. Schulz and M.J. Sundaresan

5d. PROJECT NUMBER
NREL/SR-500-40089

5e. TASK NUMBER
WER6.0301

5f. WORK UNIT NUMBER

7. PERFORMING ORGANIZATION NAME(S) AND ADDRESS(ES)
M.J. Schulz: University of Cincinnati, Cincinnati, Ohio
M.J. Sundaresan: North Carolina A&T State University, Greensboro, North Carolina

8. PERFORMING ORGANIZATION REPORT NUMBER
XCX-2-31214-01

9. SPONSORING/MONITORING AGENCY NAME(S) AND ADDRESS(ES)
National Renewable Energy Laboratory
1617 Cole Blvd.
Golden, CO 80401-3393

10. SPONSOR/MONITOR'S ACRONYM(S)
NREL

11. SPONSORING/MONITORING AGENCY REPORT NUMBER
NREL/SR-500-40089

12. DISTRIBUTION AVAILABILITY STATEMENT
National Technical Information Service
U.S. Department of Commerce
5285 Port Royal Road
Springfield, VA 22161

13. SUPPLEMENTARY NOTES
NREL Technical Monitor: Alan Laxson

14. ABSTRACT *(Maximum 200 Words)*
This report describes the efforts of the University of Cincinnati, North Carolina A&T State University, and NREL to develop a structural neural system for structrual health monitoring of wind turbine blades.

15. SUBJECT TERMS
wind turbine blade test; structural test; structural health monitoring; structural neural system; wind energy; wind turbine

16. SECURITY CLASSIFICATION OF:			17. LIMITATION OF ABSTRACT	18. NUMBER OF PAGES	19a. NAME OF RESPONSIBLE PERSON
a. REPORT	b. ABSTRACT	c. THIS PAGE			
Unclassified	Unclassified	Unclassified	UL		19b. TELEPHONE NUMBER (*Include area code*)

Standard Form 298 (Rev. 8/98)
Prescribed by ANSI Std. Z39.18